NANOSCALE DOSE DISTRIBUTION IN CRITICAL STRUCTURES OF X-RAY IRRADIATED CELL WITH EMBEDDED GOLD NANOPARTICLES: AN ANALYTICAL FRAMEWORK FOR THE ASSESSMENT OF THE CELL SURVIVAL

Submitted by

Wilmer Melo Bernal

B.Sc (Physics)

A thesis submitted in fulfilment of the requirements for the degree of

MASTER OF SCIENCE IN PHYSICS

UNIVERSIDAD DE SONORA
División de Ciencias Exactas y Naturales
Departamento de Investigación en Física
Posgrado en Ciencias (Física)
Hermosillo, Sonora
December 2014

Universidad de Sonora

Repositorio Institucional UNISON

CONTENTS

INTRODUCTION
CELL SURVIVAL

Animal cells are typically 5-20 μm in diameter. Cells are enclosed by a plasma membrane that separates the inside of the cell from its environment. The internal component of these cells are called organelles and include the nucleus. Ionizing radiation can cause breakage to this DNA strand resulting in cell death and mutation. It has been established that DNA and chromosome structure is the principal target in biological damage by ionizing radiation.

The interactions of ionizing radiation with matter, result in the production of secondary electrons and free radicals. The free radicals travel to the targets and break the chemical bonds of proteins and DNAs. The disruption of the chemical bonds will create new bonding and cross linkage between these macromolecules that will affect cells' vital function. For example, the DNA double strand structure can be broken by either single strand breakage or double strand breakage. Single strand breakage is usually easily repaired using the template from the other unbroken strand and therefore may result in minor biological consequences only if the repair is incorrect. Double strand break, however, causes significant effects leading to severe biological damage. Double strand breaks are usually irreparable and can be wrongly matched even if they undergo repair. This complete disruption leads to cell death, carcinogenesis or mutation. (Rahman, 2010)

The damage by ionizing radiation to biological matter is usually quantified by using cell survival curves. Cell survival curves represents the relationship between the radiation dose and the proportion of cells that survive irradiation as measured in vitro. The shape of the cell survival curves is dependent on factors such as the type of radiation and the cell line. It is usually described using a radiobiological model and one of the most common models used is the linear quadratic model.

The damage caused by ionizing radiation to biological materials is highly dependent on number of radiation interaction and dose deposited. Interaction of x-rays with high density and high Z materials will result into high numbers of free radicals which will cause significant damages to the DNA molecules in the cells hence leading to cell death. Therefore, if large numbers of such particles are introduced into cells in the target it will enhance radiation

effects. One mechanism lately explored for delivering high Z atoms into biological targets is nanostructures which has been mainly analyzed in this study.

Why it is needed?

At the level of absorbed doses typical of medical imaging exposures, cell death is manifested by the lack of reproductive ability. Hence, the deaths of individual cells or colonies of cells due to ionizing radiation can be readily assessed through in vitro assays. The measurement of the fraction of cells that survive following in vitro exposure to ionizing radiation is fundamental to understanding cellular radiobiology and the environment that can affect the radio sensitivity of the cell. (McParland, 2010)

In vitro measurement of a cell's response to radiation requires the excision of the tumor or tissue of interest, the fragmentation of the sample into individual cells which are then seeded into a culture dish with an appropriate growth medium and then incubated. The cell number density (number of cells per unit volume of medium) can then be measured using, for example, a hemocytometer. As a result, a given number of cells can then be seeded in a growth medium, incubated and then viewed, following staining, after a period of about 10 days. Each individual cell has the potential to be clonogenic (to grow to form a colony). The efficiency with which seeded cells eventually form colonies is defined as the plating efficiency.

What do they calculate?

In a radiobiology experiment, a number of cell cultures are formed and exposed to ionizing radiation. As each colony is the product of a single cell, the SF (surviving fraction), accounting for the plating efficiency, represents the fraction of original cells that remain viable following irradiation. It is important to recognize that the SF is not only a function of the singular absorbed dose, but also of a wide variety of radiation and environmental factors.

Hence, the bridging from in vitro experimentation to the prediction of in vivo response must account for such factors which can evolve in the in vivo environment.

A variety of mathematical models of the probability of cell lethality following irradiation were developed (the most widely used models are slightly presented in the literature review chapter). The LQ model has been extensively used in applications of clinical radiobiology to external beam radiotherapy, brachytherapy, and radionuclide therapy; reproducing an accurate fitting to the experimental obtained data of cell survival with the theoretical predicted ones, therefore we had adopted this model to develop our analysis in cell survival.

What is used to decrease the cell survival fraction?

The goal of radiotherapy is to provide tumor control by killing cancerous cells while simultaneously sparing surrounding tissues. This requires delivering high doses to tumor volumes while minimizing those to surrounding healthy tissues.

In current medical practice, this is typically achieved through spatial dose around the tumor through the use of multiple modulated radiation fields, such as Intensity Modulated Radiation Therapy (IMRT). However, the dose ratio achievable between a tumor and surrounding healthy tissues is typically limited by their very similar x-ray absorption characteristics.

Alternative methods to improve the discrimination between tumours and healthy tissue are being considered. The use of heavy atom as contrast agents has received increasing interest in recent years. Heavier elements increase the dose delivered to surrounding tissue due to their greater mass energy absorption coefficients, and can thus potentially improve the contrast between healthy and cancerous cells if they can be preferentially delivered to tumours. To be clinical useful, a radiosensitizer and/or a dose enhancer should significantly increase the therapeutic ratio and should be readily available easily used and non-toxic. These properties will facilitate the rapid translation of a laboratory effect into a clinical benefit. (Herold, Das, Stobbe, Iyer, & Champman, 2000)
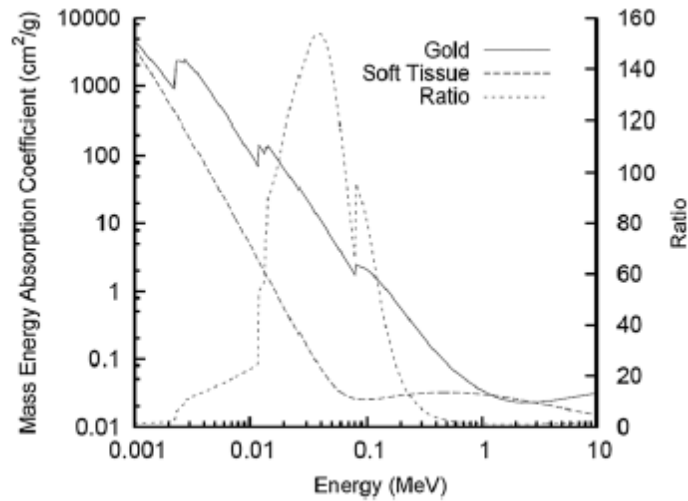
Comparison of the photon mass energy absorption coefficients for gold and soft tissue. The ratio of the mass energy absorption coefficients is shown as a function of photon energy. Image taken from (Karl Butterworth, 2012)

The use of gold nanoparticles (GNPs) as a radiosensitizing agent represents a novel approach to enhance the effectiveness of ionizing radiation. The GNP radiosensitization relies on gold's increased photoelectric absorption cross-section relative to tissue (previous figure). When irradiated, this increased local photon absorption resulting in a highly energy deposition around the GNPs, due to the localized escaping photoelectrons, Auger electrons and characteristic x-rays. A surface conjugated to tumor targeting and gold's general biocompatibility are features of GNPs that give support to the notion of GNP radiosensitization as part of a future clinical strategy. (Lechtman, et al., 2011)

This remarkable properties of gold nanoparticles allow us to consider it in our analyses as a radiosensitizer material. Accordingly to the huge amount of papers that evaluate the viability of gold nanoparticle radiation therapy and their promising results, we analyze the cell survival effects of embedded gold nanoparticles in *in vitro* cell cultures, nonetheless the analysis here presented can be extended to high Z materials nanoparticles, used as radiosensitizers.

THESIS AIMS

Nanoparticle-aided therapy is currently being considered for a number of therapeutic approaches in cancer medicine, including targeted drug delivery, photodynamic therapy, hyperthermic therapy, and radiotherapy. Gold nanoparticles (GNPs) are of particular interest in radiotherapy because their established biocompatibility and the high K-edge of gold (80.7 keV) that can lead to the emission of low- energy photoelectrons and Auger electrons upon irradiation with photons below 200 keV. Combined also with the tendency of GNPs, when administered under specific formulations, to concentrate within tumors, these properties make GNPs an attractive area of investigation for improving therapeutic ratios in radiation therapy.

This work aim to deduce analytical expression to describe the dose deposition in a critical structure with embedded gold nanoparticles and as an application of the results develop an analytical frame for the assessment of the survival of cell cultures with embedded GNPs as dose enhancers. GNPs could be studied and assessed in terms of dose enhancement, biological effects and a justification must be made of how the potential benefits of their use outweigh any risks before GNPs will be considered for clinical trials. This thesis is just such an analytical assessment of the applications of GNPs in cell survival analysis. Moreover, this thesis develops an analytical approach to describe the dose deposition in a cell target embedded with GNPs, and as an application a form of characterize the response of cell cultures with embedded GNPs after irradiation with X-rays, taking as a input the coefficients of its response to radiation of the cells (without GNPs) exposed to the same X-rays irradiation. Studies are conducted analytically and assessed by numerical evaluation to evidence its accuracy in reproduce modifications in the cell survival parameters. The specific aims of this thesis are as stated below:

- To simplify an expression for the dose deposited around a single GNP suspended in water-like tissue after irradiation under certain conditions and compare the accuracy of the proposed expression.

- To develop an analytical description of the dose deposition inside a critical structure (cell) for certain cases of GNP distributions (single GNP centered in the cell, GNP outside the cell, GNPs inside the cell).

- To compare the calculations of dose deposited in a cell structure from two different perspectives; the spatial r-domain and the dose D-domain standing out the potentiality of the analysis in each domain and identifying the one who provides a wider application at the time of assess in real scenarios.

- To provide an analytical description of the radiobiological effects of GNPs on cells using as input the analytical expression for dose deposition proposed. In this study, the LEM radiological model will be used to predict the response of a cell culture after irradiation when it had embedded gold nanoparticles and the local dose at each point of the cell structure is known. To derive the formulas to calculate the linear quadratic parameters (alpha (α) and beta (β)) that reproduce the response of the cell survival curve with embedded GNPs.

- To verify the accuracy of the analytically estimated LQ parameters with the *in vitro* experimentally measured ones. And identify possible modifications of the presented model to improve the veracity of the analytically estimated values.

CHAPTER I. LITERATURE REVIEW.
1.1 RADIATION DAMAGE IN CELLS.

In radiotherapy, ionizing radiations are targeted to tumours, a category of biological tissue and therefore a living organism. The interaction of ionizing radiations with biological structures results in cell or tissue damage. If the damage is unrepairable, cell death will occur.

Animal cells are typically $5 - 20\mu m$ in diameter. Cells are enclosed by a plasma membrane that separates the inside of the cell from its environment. The internal components of these cells are called organelles and include the nucleus. It contains most of the cell's genetic material, organized as multiple long linear DNA molecules in complex with a large variety of proteins, to form chromosomes. Ionizing radiation can cause breakage to DNA strand resulting in cell death and mutations. It has been established that DNA and chromosome structure is the principal target in biological damage by ionizing radiation.

The interaction of ionizing radiation with water or tissue, results in the production of secondary electrons and free radicals. The production of secondary electrons and free radicals can be categorized as the result of a direct action or an indirect process. Direct action usually involves high linear energy transfer (LET), such as neutrons and alpha particles. In this process, the ionizing radiation directly interacts with the targets, causing atoms to become ionized and excited. An atom in an ionized and excited state can be considered as a free radical that will interact with other atoms and produce a chain of biological effects. Indirect action occurs when ionizing radiation interacts with other atoms and molecules, such as water and induces the production of free radicals. The free radicals will the travel to the targets and break the chemical bounds of proteins and DNAs. For example, the DNA double strand structure can be broken by either single strand breakage or double strand breakage. Single strand breakage is usually easily repaired using the template from other unbroken strand therefore may result in minor biological consequences, the repair system is essential for living cells to survive in oxidative circumstances since oxidative DNA damage is constantly produced by oxygen radicals generated in the physiological process of energy production. (Kobayashi, Usami, Porcel, Lacombe, & Sech, 2010). Double stand breaks are usually irreparable and can be wrongly matched even if they undergo repair. This complete disruption leads to cell death, carcinogenesis or mutation. (Rahman, 2010)

The damage caused by ionizing radiation to biological materials is highly dependent on number of radiation interaction and dose deposited. The interaction of x-rays with high density and high Z materials will result into high numbers of free radicals which will cause significant damages to the DNA molecules in the cells hence leading to cell death. Therefore, if large numbers of such particles are introduced into cells in the target it will enhance radiation effects. One mechanism lately explored for delivering high Z atoms into biological targets is the use of nanostructures; an analysis of its energy deposition after irradiation with x-rays is the main aim in this study.

When x-rays photons interact with matter, the first mechanism that is activated is either photoelectric absorption or a Compton effect. These ionization events of molecules correspond to the energy deposition events in matter. More importantly, the electrons emitted either by photoelectric effects or by Compton effects can further induce energy deposition in matter until these ionization events totally exhaust their kinetic energy. The range of energetic Compton electrons might be up to several hundred microns. In cases of lower energy, of photoelectrons or Auger electrons, however, the range size becomes much smaller; the range of $1 keV$ electron is calculated around $0.05 \mu m$. Energy deposition events are produced along these tracks, and radiation energy is thus distributed in the biological system. These physical events initiate biophysical processes in the irradiated system. For this reason, radiobiological phenomena are assessed on the basis of the energy deposited in the biological system, hence, the metric Gy (Gray) is defined as the energy (J) deposited divided by the mass (kg) of the system concerned. This quantity corresponds to an averaged value in the target, and is not a sufficient basis upon which to predict the resulting radiobiological phenomena.

In radiation biology, it is important to relate the radiation energy deposited by these physical processes to the resulting radiobiological phenomena from the viewpoint of the amount of energy deposited per event, as well as the spatial distribution of these events along the track of the charges particle. In aqueous systems that include living cells, the indirect effects mediated by radicals are known to play an important role in the production of DNA damage. These radicals can react with various molecules in an aqueous solution due to their high reaction coefficients. This determines the diffusion lengths of radicals, or the lifetime of

radicals. Diffusion lengths can be calculated as several 10 of nm in intracellular circumstances in which many kinds of biomolecules are dissolved. These suggest that energy deposition events and consequently Auger effects need to occur very close to biologically important molecules such as DNA. Therefore it has generally been believed that localization in the nucleus gives higher sensitization due to the higher resulting efficiency in producing DNA damage.

1.2 DOSE DISTRIBUTION AROUND X-RAY IRRADIATED GOLD NANOPARTICLE

1.2.1 Monte Carlo Simulations.

Recently, Monte Carlo (MC) simulations have been used to investigate the dose enhancement from gold nanoparticles within microscopic $(nm - \mu m)$ distances in response to clinical x-ray beams, brachytherapy sources and low energy gamma- / x-rays. The dose enhancement was characterized via considering numerous interaction phenomena and quantities, such as photoelectric absorption, properties of secondary electrons ejected from GNPs, photoelectric energy conversion, as well as dose ratios.

For a single GNP the spatial distribution of DER is found to be nearly isotropic with limited magnitude and relatively short range (100-200 nm for DER significantly greater than 1). For a cluster of GNPs both the magnitude and range are found much greater $(1 - 2\mu m)$. The relation between DER for clusters of GNPs and a single GNP is strongly nonlinear. (Zygmanski, et al., 2013) The nonlinear relation between DER for a single and multiple GNPs suggest that parameters such as the number of adjacent nanoparticles per cell and the distance between the GNPs in the cellular target may be important in assessing the biological effectiveness associated with GNP.

Due to various limitations in the MC method, simulations of energy deposition at submicroscopic (or nanoscopic) levels must be carried out separately from the simulation at macroscopic $(mm - cm)$ levels. Due to those limitations in most of the simulations a well-known technique in multi-scale radiation transport simulations is used in this technique two stages are necessary. Figure 1.1. In the first (macroscopic) stage of the simulation the x-rays

are transported across macroscopic depths (mm to cm) to a location near the target GNP in a homogeneous medium where the phase space is determined. Phase space incorporates all particle types, their numbers, energy and direction of motion. In the second stage, this phase space (spectrum) is used as the source for a new MC simulation to determine the nanoscopic dosimetric quantities. Therefore a bridge between the two levels (macro-micro) has to be established. Modeling the transition between the macroscopic and nanoscopic levels of simulation is essential in order to ensure that the magnitude of the computed dose enhancement effects is not misrepresented. (Zygmanski, et al., 2013). DER is defined as the local energy deposited within a microscopic voxel in the medium near the GNP (or multiple GNPs) divided by the energy deposited in the same voxel without the presence of GNPs. The microscopic scoring voxel size in the proximity of GNPs is the volume where the DER is estimated, depends on the aims of the analysis the scoring voxel size ranges from micrometers to nanometers.
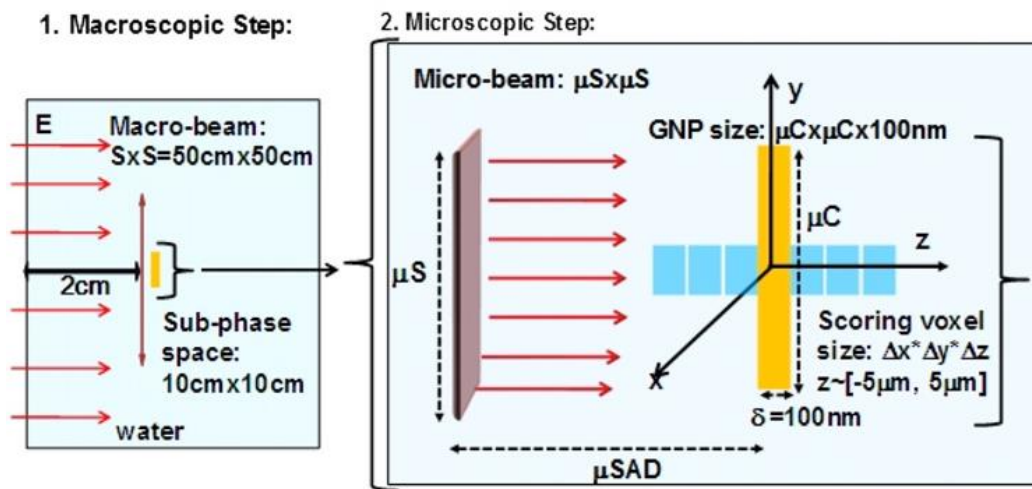
Figure 1.1 Schematic diagram (example) of the macroscopic and microscopic simulation geometries for a single gold nanoparticle of varying size, the scoring voxel are placed near the GNP. Adapted from Zygmansky (2013)

In real experiments the most likely morphology is a cluster of nanoparticles rather than solitary nanoparticles. Owing mostly to self-shielding and nanoparticle packing geometry within the cluster, the dose distribution about the cluster of nanoparticles cannot be obtained by superimposing dose distributions due to many single nanoparticles. The dose to the

cellular or sub cellular target is therefore a nonlinear function of the number of particles and their morphology.

The difference in the photoelectron fluency between the cases with and without GNPs is more pronounced below the electron energy of about $20keV$, due to the increased photon interactions around gold $L-$ and $M-$ shell photoelectric absorption edges. (Cho S. , Jones, Krishman, & Sunil, 2009) The photoelectrons contribute to the local energy deposition significantly more than the Auger electrons, even though the fluence of the photoelectrons is comparable to that of the Auger electrons. However, the role of Auger electrons, particularly those with large abundance due to gold $L-$ and $M-$ shells relaxation processes, would become significant when one considers microscopic dose enhancement for the current cases on a cellular level to find some correlation with radiobiological effects.
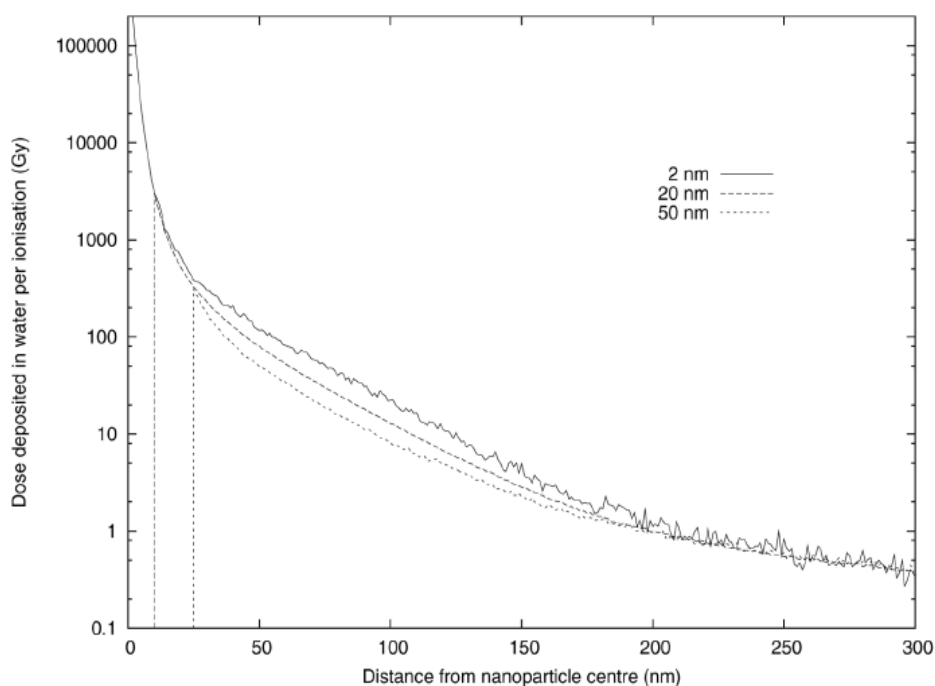
Figure 1.2. Average radial dose which are deposited following a single ionizing event from 40keV primary radiation in gold nanoparticle of variety of sizes. Areas in the vicinity of the nanoparticle, see extremely large doses following a typical ionizing event. Small nanoparticles deposit more in their local area than larger ones, due to the greater relative contribution from the outer layer of the nanoparticle.Adapted from (McMahon, 2011)

The average dose deposited assessed in MC calculations in the vicinity of a $2nm$ GNP following a single ionizing event by a $6MV$ source is shown in the Figure1.2. It shows that, as in kilovoltage irradiations, single ionizations in a GNP have the potential to deposit very

high doses in the surrounding water volume due to the cascade of low-energy secondary electrons generated following an ionizing event in gold. The consideration of these dose inhomogeneities in dose will lead to predict levels of radiosensitization which are substantially greater than macroscopic dose enhancement, as observed experimentally.

The analysis of MC calculations conclude that dose enhancement is found to be almost isotropic about a spherical GNP but its magnitude strongly depended on the simulation micro-geometry (model of the micro source) and the phase space properties (plane-parallel versus full angular phase space). Under non-uniform GNP distribution (the number of GNPs and their distance to specific cellular targets) such stochastic effects may lead to decreased radiobiological effectiveness of GNP therapy.

1.2.2 Analytical Approach: Dose distribution in cells.

Most works have focused on the macroscopic dose enhancement averaging effects over volumes much larger than a single NP. Approach that is fundamentally flawed because it ignores the significant dose inhomogeneity in the vicinity of embedded NPs. Monte Carlo (MC) simulations gives an alternative view on NP radiosensitization, this are carried out to calculate dose in the nanoscale vicinity of individual NPs. Despite the fact that MC methods provide precise numerical results, it is desirable to have and analytical solution that, will unavoidably simplify the physical model, and would provide valuable insight into the nature of the studied problem and gives a possibility to alter parameters and conditions without having to rerun costly MC simulations. Few papers present advances in describe analytically the dose deposition around nanoparticles or the dose enhancement due to its presence in media.

Some published papers present an analytical approach to calculate the dose enhancements in cells and their nuclei due to the presence of gold nanoparticles around them. The location relative to nuclei and the gold nanoparticles concentration are one of the most important variables considered in this studies. These analysis consider the contribution from photoelectrons and Auger electrons in order to develop an accurate calculation of the micro-scale dose enhancement.

Endothelial cells are the selected ones in these analysis to perform the calculations. Tumor endothelial cell damage during radiation therapy contribute significantly to tumor eradication and treatment efficacy. Preclinical research has established that combining tumor vascular disrupting agents (VDAs) with radiotherapy results in consequential improvements in cancer treatment outcome. The vascular disrupting agents cause vascular shutdown leading to extensive ischemic necrosis in the core region of the tumor. The vascular shutdown caused by VDAs leads to the destruction of large tumor areas in the central tumor region, including hypoxic areas typically most resistant to radiation. (Ngwa, Makrigiorgos, & Berbeco, 2012)

Given that GNP can be concentrated or located selectively to the tumor endothelium via its functionalization, and that photoelectrons generated in gold have inherently very short ranges, localized effect and a boost of radiation dose to endothelial cells in the vicinity on GNPs is expected. The studies used cellular microdosimetry to calculate local radiation dose enhancement by vasculature confined GNPs during irradiation by brachytherapy sources, 6 MV Linac beam and $50\ kVp$ x-rays. They considered ranges of GNPs concentrations as reported in literature, and assume that GNPs are confined to the tumor vasculature. A simple geometric model to calculate the local energy loss of photoelectrons and/or Auger electrons originated from the nanoparticles on the endothelial cell surface was used Figure1.1.

In the following paragraphs a short review of the procedures, considerations and calculations developed in the published papers related with endothelial dose enhancement due to GNPs aided radiotherapy is presented.

The tumor vascular endothelial cell was modeled as a thin slab with dimensions of $2\mu m$ (thickness) $x\ 10\mu m$(length) $x\ 10\mu m$(width). A spherical nanoparticle is simulated to be attached to the vascular-side surface of the endothelial cell. (Berbeco, Ngwa, & Makrigiorgos, 2011) A nucleus is added with 5% to 10% of the cellular volume, corresponding to typical nucleus dimensions and sizes. (Ngwa, Makrigiorgos, & Berbeco, 2012) (Hossain & Su, 2012) Figure1.1 illustrates a simplified model of the endothelial cell and nucleus which is assumed to be centrally located. The exact position of the GNP is not of particular importance as several nanoparticles, assumed to be evenly spread along the lumen wall of the vasculature, can be attached on a single endothelial cell. Furthermore photo/Auger electrons from nanoparticles attached near the edge of an endothelial cell may

deposit energy to the adjacent cell, and vice versa, thereby providing lateral electron equilibrium. Such lateral compensation of the emitted energy allows energy emission from GNPs in the periphery of endothelial cells to be treated similar to centrally located GNPs.
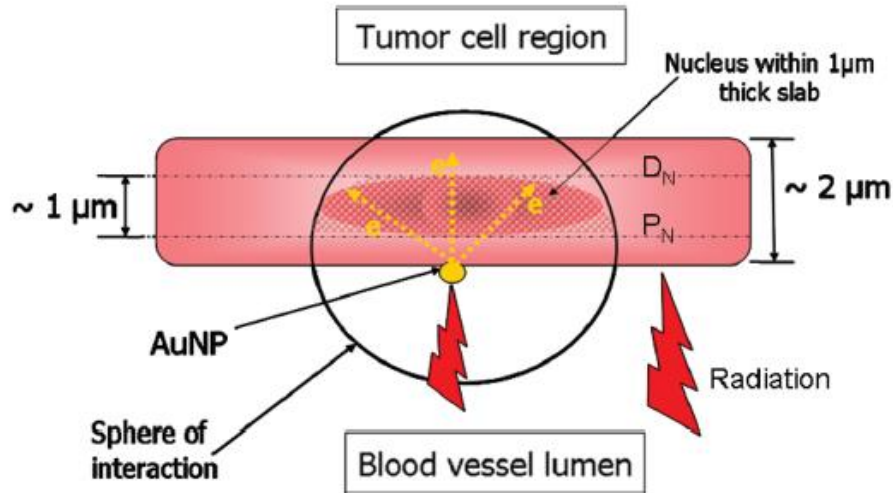
Figure1.1 Simplified model of an endothelial cell. The gold nanoparticles are attached to the vascular-side surface of the cell. The range of electron is shown as a sphere of interaction, with the nanoparticle at the center. (adapted from Ngwa 2012)

For the estimation of the dose enhancement an arbitrary dose D_w is taken as the dose absorbed by the cell without nanoparticles, the choice of the authors was a dose of $2Gy$ (the choice of a different dose will lead to the same results due to the definition of the DEF (dose enhancement factor))

The calculations evaluate the energy deposited by a single created photoelectron at the surface of the GNP deposited in the slab cell structure, then the same value is prescribed for all the created electrons in the case of monoenergetic irradiation; the self-attenuation due to GNP dimensions is not taken into account. The total number of emitted photoelectrons is calculated as the product of the number of photoelectrons created by a single nanoparticle, multiplied by the total number of nanoparticles.

To evaluate the range of emitted photoelectrons, the kinetic energy E_{KE} of emitted photoelectrons must be known, it is given by $E_{KE} = E - E_{edge}$, where E_{edge} is relevant photoelectric absorption edge of nanoparticle. As emitted photoelectrons interact with their surroundings, they will deposit energy in a sphere of interaction centered on the nanoparticle, the sphere represent the possibility of an arbitrary direction of ejection of the photoelectron,

which moves in a straight path. The radius of interaction sphere defines the range R_{tot} of photoelectrons given by

$$R_{tot} = 0.0431(E_{KE} + 0.367)^{1.77} - 0.007 \quad (1.1)$$

The last expression gives the total range of a photoelectron generated in the surface of the GNP moving in water measured in μm, the value of the energy should be expressed in keV. The papers use the Cole's empirical relation between electron energy loos $(dE_{KE})/(dx)$ and range $R_{tot}(\mu m)$

$$\frac{dE_{KE}}{dx} = 3.316(R_{tot} - x + 0.007)^{-0.435} + 0.0055(R_{tot} - x)^{0.33} \quad (1.2)$$

Where x is the distance from photoelectron emission site. Each photoelectron emitted from an NP will deposit energy locally as a function of its initial kinetic energy. The energy deposited within the volume of interest (whole cell or cell nucleus) is calculated by integration over the differential energy loss (dE/dr) from the closes surface of the volume of interest to NP, to the farthest surface of the volume of interest. In the integration the hemispherical shell in the blood vessel is excluded, as the spherical shell beyond the volume of interest of the endothelial cell. Therefore the energy deposited within the endothelial cell is calculated as

$$E_{EC} = \int_r^{R_{tot}} \frac{A_h - A_{hc}}{SA} \cdot \frac{dE_{KE}}{dx} dx \quad (1.3)$$

Where A_h is the area of the hemisphere that intersects the cell, A_{hc} is the area of the hemispherical cap beyond the endothelial cell and SA is the surface area of the entire sphere. (To clarify see the sphere of interaction in Figure1.1)

Rewriting the equation replacing the areas of the integral we get (Hossain & Su, 2012)

$$E_{EC} = \int_r^{R_{tot}} \frac{2\pi R_{tot}^2 - 2\pi(R_{tot} - t)R_{tot}}{4\pi R_{tot}^2} \cdot \frac{dE_{KE}}{dx} dx$$

$$(1.4)$$

The lower limit of the integration is the radius of the nanoparticle and the upper limit is the total range of the photoelectron (the final radius of the sphere of interaction). Assuming a homogeneous distribution of nanoparticles, and dose deposited in the entire sphere of

interaction, the total energy deposited to cell E_{EC} by photoelectrons can be derived by multiplying by the number of emitted photoelectrons (monoenergetic case); that is

$$E_{ECtotal} = E_{EC} \cdot N_{PEtotal}$$

The absorbed dose is given by the energy deposited in the endothelial cell divided by its mass. It is assumed that each neighboring endothelial cell has a similar nanoparticle attached: therefore energy that is deposited in an adjacent cell (cross-fire) is accounted (Ngwa, Makrigiorgos, & Berbeco, 2010). Dose delivered to the entire cell by photoelectrons following nanoparticle and x-ray interactions is obtained by

$$D_{NP}(PE) = \frac{E_{ECtotal}}{V_{EC} \cdot \rho_{EC}}$$

and as it is defined, the DEF due to photoelectrons is given by

$$DEF(photoelectrons) = \frac{absorbed\ dose\ with\ nanoparticles}{absorbed\ dose\ without\ nanoparticles} = \frac{D_w + D_{NP}(PE)}{D_w}$$

remarking that DEF of 1.0 refers to 0% enhancement, whereas a DEF of 2.0 refers to 100% enhancement.

To derive contributions from Auger electrons, Auger electrons spectra obtained from Monte Carlo simulations for tumors loaded with gold nanoparticles and irradiated with certain sources (Cho, Jones, & Krishnan, 2009) were used by the authors. The energy deposited by Auger electrons in the cell was determined as described for photoelectrons. The product of number of source photons and number of Auger electrons per source photon gives the total number of Auger electrons emitted. The total energy deposited for each energy beam equals the number of Auger electrons emitted multiplied by the corresponding energy deposited. Summing over all energy beams then yields to the total energy deposited in the endothelial cell.

The results for the endothelial dose enhancement, due to GNPs emitted photoelectrons and Auger electrons, as a function of local concentration obtained by (Ngwa, Makrigiorgos, & Berbeco, 2010) are presented in Figure 1.2 as it is expected, the EDEF increases with the GNP concentration.
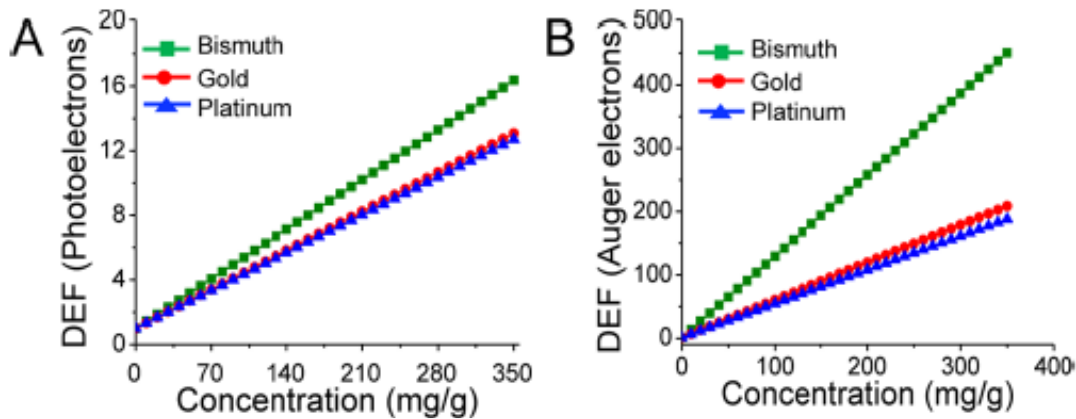
Figure 1.2 A) Endothelial dose enhancement factor (EDEF) as a function of local GNP concentration at the endothelium due to photoelectrons. Auger electrons are not included in the calculation of the EDEF B) Endothelial cell dose enhancement factor (EDEF) as a function of local nanoparticle concentration due to Auger electrons, both calculations were made for 400 nm diameter bismuth, gold and platinum nanoparticles irradiated by a 50kVp external beam x-ray source. Adapted from (Hossain2012)

Although, EDEFs due to Auger electrons increase linearly with nanoparticle concentration, they are considerable higher than dose from photoelectrons at the same concentration. As a result of the near-particle energy deposition, dose contribution within several hundred nanometers from nanoparticle location is dominated by Auger electrons.

The authors mentioned the fact that the calculated dose deposited in the endothelial cells and cells nucleus by these photo/Auger electrons represented average dose estimates. In particular, for lower concentrations, stochastic effects may be important. The results published predict that using GNPs in conjunction with conventional or hypofractionated radiotherapy can result in a very significant enhancement of local dose and biological effect in the tumor endothelium. This boost of microvascular dose would be expected to enhance vascular shutdown in tumors, thereby also boosting secondary tumor cell death due to ischemia.

Some facts to criticize of the papers that estimates the enhancement due to Auger electrons are first the arbitrary interpretation of the data obtained for (Cho, Jones, & Krishnan, 2009). Even when the paper gives a value of the average number of Auger electrons, created per photoelectric event, the energy of the Auger electrons is not specified at all. Another thigh to consider is the fact that enhancement factor due to Auger electrons decreases with increase in particle size. Following an ionizing event, photo or Auger electrons must escape nanoparticle before causing damage to surrounding cells; however, the percentage of

electrons emitted from nanoparticle upon x-ray excitation strongly depends on particle size, with majority of low-energy and short-range Auger electrons being absorbed more readily within nanoparticle of increasing size.

During the literature review a modification of this calculations was proposed in order to consider the effect of range and energy attenuation of photoelectrons in the equation (1.3) without taking the first term of the integral as a merely geometric constant. Congruent results were obtained providing physical meaning of all the terms of the expression (1.3). Due to the extension of the calculations and the small relevance in the context of the present analysis its presentation was omitted.

1.3 MODELS OF CELL SURVIVAL.

1.3.1 Lea's target theory.

This model was first developed in 1946, is one of the earliest interpretative models for radiation-induced cell killing and was developed starting from data on microorganisms and bioactive molecules. According to the model, which is specific for low LET radiation (providing that interaction between distinct events is rare), a cell contains one or more sensitive targets of size v, which can receive one or more radiation "hits", a hit is an "active event" occurring within the volume v, that is an energy absorption event able to induce biological damage such as an ionization or an excitation in the target molecule or in water. The hit probability is then $\rho = v/V$, where V is the total cellular volume (product between average cell volume and number of cells at risk). If D is the total number of active events in the cell population, introducing a function $H(h)$ representing the probability that the cell will survive h hits ("hit-survival function"), the survival probability after h hits is

$$P(\rho, h, D) = H(h)p(\rho, h, D) = H(h)\rho^h(1-\rho)^{(D-h)} {}_DC_h \quad (1.5)$$

where ${}_DC_h$ is the binomial coefficient expressing that h hits and $(D-h)$ "misses" can be assigned for D active events. (Ballarini, 2010). Since a cell may survive for $h = 1,2,3, ... , D$, the total survival probability for the cell, that is the general survival equation according to Lea's theory, is

$$S(\rho, D) = \sum_h P(\rho, h, D) \quad (1.6)$$

The target theory model of cell survival is based on the concept that a number of critical targets have to be inactivated for cells to be killed. The case that found widest applicability in radiobiology is the "multitarget-single-hit" (MTSH) version, according to which the cell contains n critical targets, each target has the same probability q of being hit by radiation, and one hit in a given target is sufficient to inactivate that target, not the entire cell. The probability that a cell will survive with b hits is then

$$P(q, b, n, D) = (1 - e^{-qD})^b (e^{-qD})^{n-b} \, _nC_b B(b) \quad (1.7)$$

where $B(b)$, analogous to $H(h)$, is the hit survival function. In the MTSH case, the following limiting conditions can be assigned to $B(b)$: (1) if $b < n$, $B(b)$ assumes a value so that $P = 1$, (2) if $b \geq n$ $B(b) = 0$ and $P = 0$. This means that for $b < n$ the cell will survive, whereas for $b \geq n$ the cell will die.

If the cell contains more than one identical target, each of which must be inactivated by a single hit in order to inactivate the cell, survival is represented by the multitarget, single-hit survival equation. Since the nth hit assumes nonsurvival, the overall survival probability is

$$S(q, n, D) = 1 - (1 - e^{-qD})^n$$

When lnS is plotted versus D, except for the case of $n = 1$, this equation gives a survival curve with a shoulder at low doses, that increase in breath with n; and straight-line response at higher dose. For S values below about 0.1 each curve becomes a straight line, Except for $n = 1$, the slope at zero dose will be zero, which is one of the main limitations of the model because it is not consistent with the experimental data. Survival data is usually plotted on semi-log coordinates. Target theory and the derivation of simple cell-survival relationships in terms of targets and hits dominated radiobiological thinking over a long period. A problem with this concept is that specific radiation targets have not been identified in mammalian cells. What is now understood in the importance of DNA strand breaks and of strand-break repair, the sites of damage and repair being dispersed throughout the cell nucleus. (Lehnert, 2007)
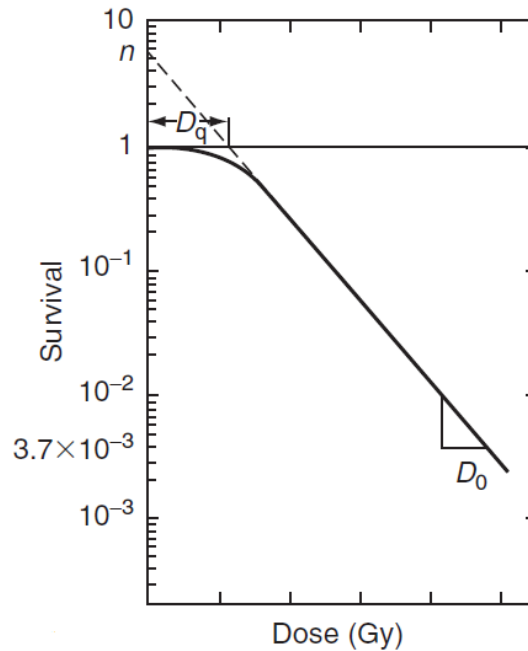
Figure 1.3 Survival curve for mammalian cells; multitarget survival curve from target hit theory. Adapted from (Lehnert 2007)

The model predicts that the slope of the linear portion of the plot remains constant with increasing dose whereas a more frequent experimental observation is a constantly increasing slope. This lead the investigators to try alternative approaches, also basing on the fact that the reported data on mammalian cell lines were better described by functions in which the dose appeared both to the first and to the second power of the prescribed dose.

1.3.2 The molecular (or linear-quadratic) model.

The target theory makes no assumption about the induction and repair of the initial DNA damage, which is now known to play a fundamental role of radiation-induced clonogenic death. A number of alternative approaches to Lea's theory have been developed to respond to such objection, and several of these approaches are of a linear-quadratic form. In 1981 Chadwick and Leenhouts developed what they called the "molecular model", which has come to be widely known as the "linear-quadratic" (LQ) model. According to the LQ model, the cell contains certain critical molecules, assumed to be double-stranded DNA, the integrity of which is essential for clonogenic survival, the critical damage is assumed to be a DNA double-strand break (DSB). Ionizing radiation can induce the rupture of DNA molecular bonds ("lesions") that, under certain conditions, are repaired, varying degrees of repair imply

different radiobiological effects. If No is the number of DNA molecular bonds available for rupture in the target cell, N is the number of these bonds that remain intact after a dose D, and k is the rupture probability of a single bond per unit dose, then

$$-\frac{dN}{dD} = kD \ , N = N_0 e^{-kD} \quad (1.8)$$

The number of effective broken bonds is therefore

$$N_0 - N = f N_0 (1 - e^{-kD})$$

where f is the fraction of broken bonds that are not repaired.

According to Chadwick and Leenhouts, the double helix can undergo a DSB as the result of two different mechanisms:

i.   Both DNA strands are broken by the same radiation track (or "event").
ii. Each strand is broken independently, but the breaks are close enough in time and space to lead to a DSB.

Let Δ be the fraction of dose acting through mechanism (i), and $(1 - \Delta)$ the fraction of dose acting through mechanism (ii). The average number of lethal DSB per cell is

$$Q = p \left[\chi \left(1 - e^{(-k_0 \Delta D)} \right) + \rho \left(1 - e^{-k(1-\Delta)D} \right)^2 \right] \quad (1.9)$$

where p is the assumed proportionality constant between the DSB yield and cell death. Since according to Poisson-type cell killing the probability of cell survival S is given by the probability of having 0 lethal lesions, then $S = e^{-Q}$. Assuming that k and ko are quite small, one gets the familiar linear-quadratic relationship as follows.

$$S = \exp(-\alpha D - \beta D^2) \quad (1.10)$$

where $\alpha = \alpha(f_0, k_0, \Delta)$ and $\beta = \beta(f_0, E, k^2, (1 - \Delta)^2)$. This model represents an attempt to bridge the gap between physics, that is energy deposition by radiation, an biology, that is DNA repair or lack of repair, although the fundamental assumptions are not widely accepted, in particular the hypothesis that the yield of DSBs is proportional to the yield of lethal lesions is not consistent with most experimental data, which in general show that DSB tend to increase linearly with dose whereas lethal lesions increases with dose in a linear $-$ quadratic fashion. However, the LQ model is widely used in radiobiology since it fits mammalian cell

survival data pretty well, overcoming not only the problem of zero slope at zero dose, but also the problem of constant slope at high doses. (Ballarini, 2010)

The linear quadratic model has taken precedence as the model of choice to describe survival curves. For doses used for fractioned radiotherapy, the LQ model adequately represents the data. The model can be manipulated to predict response to fractionated radiation and it has the advantage of depending on only two unknown factors, α and β (Lehnert, 2007)
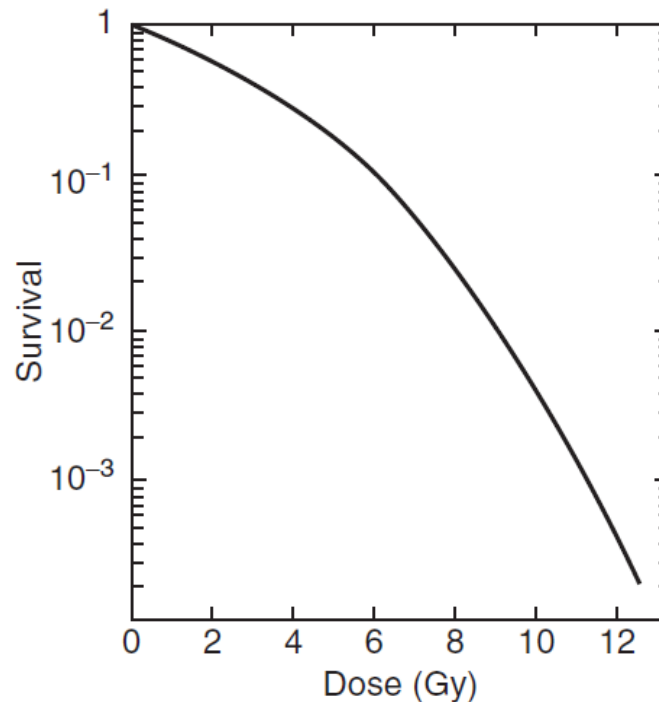
Figure 1.4 Survival curve for mammalian cells. Linear quadratic model of cell killing. adapted from (Lehnert 2007)

1.3.3 The local effect model (LEM)

A more recent approach, is the "Local Effect Model", this model is based on the assumption that the local biological effect, that is the damage in a small sub volume (nm) of the cell nucleous, is solelay determined by the expectation value of energy deposition in that sub volume, independent of the radiation type, in other words the biological effect of radiation is determined entirely by the spatial local dose distribution inside the cell nucleus. This implies that differences in the biological action of charged beams should be attributed to the different pattern of energy deposition by heavy charged particles with respect to photons, which is

radiation track structure at the nm scale. Furthermore, for a given radiation type, differences in the photon response for different biological targets should lead to differences in the corresponding RBE values. (Ballarini, 2010)

The LEM is based on the assumption that the response of cells to inhomogeneous radiation dose on the micro-scale is similar to the response of the cell population as a whole to sparsely ionizing radiation, which deposits dose uniformly throughout the cell. By summing the effects of the dose at each point over the entire cell volume, a prediction can then be made of the probability of cell death.

The local effect model uses the concept of "lethal" event, where each lethal event or lesion leads to cell inactivation. It is not relevant how these events occur, since we get the information about the probability of cell death and the corresponding average number of lethal events from experiments with x-rays. In these experimental data, all kinds of damages such as complex strand breaks or DNA misrejoining as well as the repair mechanisms are included. Therefore, a lethal event may also be the result of several sublethal damages that in combination lead to cell inactivation. (Elsässer & Scholz, 2007)

According to LEM, the biological characteristics of the various target tissues are essentially determined by the α/β ratio for conventional photon irradiation. Moreover in cell- survival analysis, the fraction of cells which survive an exposure to ionizing radiation is given by a linear-quadratic response,

$$S = e^{-(\alpha D + \beta D^2)}$$

where α and β are characteristics of the cell line, and D is the mean dose delivered to the entire volume containing the cells. This dose is typically calculated on a macroscopic scale, averaged over a volume containing a very large number of cells.

This approach works well for sparsely ionizing radiation such as the X-rays which are typically used in radiotherapy. However, if an equal dose D is delivered to a cell population using densely ionizing radiation such as heavy ions, significantly more cells are killed. This increase in killing is referred to as the Relative Biological Effectiveness (RBE). While the RBE can be empirically determined from cell survival experiments, considerable effort has also been put into explain it from a theoretical basis. One such approach which seeks to do

this is the Local Effect Model (LEM). Instead of considering the cell-killing effects of an average macroscopic dose as described above, the LEM considers the probability of damage occurring at each point in a cell based on the dose at that point alone, and calculates a surviving fraction based on the sum probability of damage occurring over the whole cell. (McMahon S. , et al., 2011)

The LEM describes the damage which occurs to cells in terms of "lethal lesions" which can be described in the case of a uniform dose as

$$S(D) = e^{-N(D)} \quad (1.11)$$

where $N(D)$ is the number of lethal lesions induced by a homogeneous dose D. Lethal lesions are not explicitly characterized, but are simply defined as any event which lead to cell death. Thus, for sparsely ionizing radiation, it can be seen that applying the linear-quadratic the number of lethal lesions is

$$N(D) = \alpha D + \beta D^2 \quad (1.12)$$

However, for inhomogeneous radiation, the number of lesions induced is calculated based off the local dose at each point and then integrated over the whole cell volume, giving

$$N_{tot} = \int N(D(r)) \frac{dV}{V} = \int (\alpha D(r) + \beta D(r)^2) \frac{dV}{V} \quad (1.13)$$

where $D(r)$ is the local dose delivered at point r, and dV/V is the corresponding volume fraction which sees that dose. Once the total number of lesions within a cell, N_{tot}, is calculated, the survival probability is then given by

$$S_{LEM} = e^{-N_{tot}} \quad (1.14)$$

It can be seen that this simplifies to the standard survival curve in the case of a uniform dose, but inhomogeneous doses can cause grater levels of damage due to quadratic term in the dose response. While the LEM is typically applied to heavy ion therapies, it can be applied to any system where the dose distribution can be calculated, such as the GNP-radiation interaction.

Once the rapidly-varying component of the dose distribution has been calculated, this can be added to the effectively uniform background dose level which is delivered by x-rays which do no interact with GNPs to give the full dose volume distribution for a given combination of x-ray energy and GNP size. This can then be applied to the function above to calculate the local damage at each point in the volume, and thus N_{tot} and S_{LEM}.

This model requires three input quantities: (i) the volume V of the sensitive target, (ii) the local dose distribution d and (iii) the experimental survival curve S after irradiation. In the present analysis the LEM theory of cell survival was used to exemplify the potential uses of the analytical framework for radial dose distribution in cell structure proposed.

1.4 SIMULATED CELL SURVIVAL CURVES FOR CELL CULTURES WITH EMBEDDED GOLD NANOPARTICLES.

There are a few papers who describe analytical or simulation efforts to predict cell survival of cell cultures with embedded gold nanoparticles after irradiation with x-rays. This papers present as a goal starting from the calculation of the dose distribution on the nanoscale in the vicinity of the GNPs, introduce a model for cell survival which can take this inhomogeneities into account to generate new predictions for the effects of GNP on radiotherapy and in the cell survival analysis. Therefore analyses whether the dose inhomogeneities created by the GNPs on a sub − cellular scale affect the non-linear dose dependence of cell survival.

The papers highlighted the discrepancy between the theoretically predicted increases in cell killing and experimentally observed results. Theoretical studies suggest that GNP concentrations on the order of 1% combined with keV x-rays would be necessary to generate significant increases in cell killing, experimental studies have observed enhancement of the effects of radiation at GNP concentrations which are orders of magnitude smaller. On the other hand, due to the lack of contrast between tissue and gold, these models predict little benefit at the megavoltage energies typically used in therapy; however, in vitro experimental studies of GNP radiosensitization present a rather different picture, with many reporting radiation sensitizing effects substantially greater than the additional dose due to the presence of GNPs.

The theoretical and simulated calculations of these papers where compared with in vitro results previously published. The MDA-MB-231 cells where chosen from the calculations. The procedures of preparing the cultures and the embedding of GNP are described in (McMahon S. , et al., 2011) with the irradiation procedures and the measures of cell uptake with the TEM.

To estimate the dose enhancement in the cellular targets due to the presence of GNPs Monte Carlo calculations where performed by the authors. The dose distribution in the GNP-water system is typically calculated by scoring energy deposits in concentric shells centered on the gold nanoparticle and dividing these deposits by the mass of the shell. However this calculation is misleading, as energy deposits spread from the location of the ionizing events, rather than the nanoparticles center Figure 1.5. As a result, calculations of dose which center on the nanoparticle tend to slightly underestimate dose, by considering energy deposits spread over a large than is actually the case.
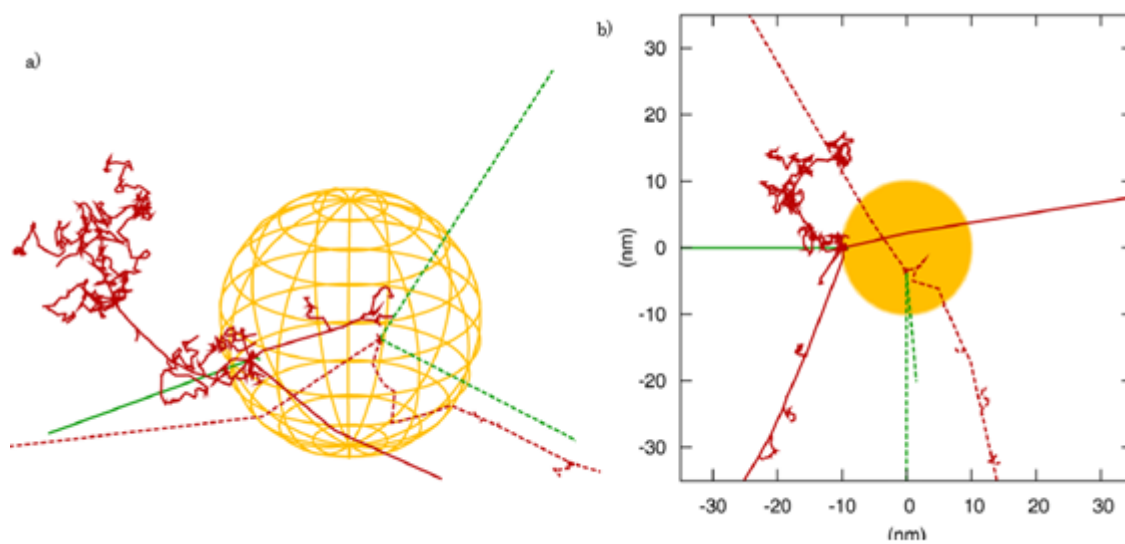

Figure1.5 Comparison of track structure of ionizing events either on the surface (solid lines) or in the bulk (dashed lines) of a 20nm spherical gold nanoparticle, plotted both in 3D (a), and as a 2D projection (b). Adapted from (McMahon, 2011) In the figure, an incident 50keV photon (green tracks) interacts with the gold nanoparticle and ejects a number of electrons (red tracks). For the event which occurs in the bulk, the majority of low-energy electrons are stopped immediately in the nanoparticle allowing only the most energetic and sparsely ionizing electrons to escape. By contrast, the surface event also produces a very large shower of low energy electrons who deposit their energy very densely in the vicinity of the nanoparticle, leading to high doses and many ionization events in a small volume.

The dose distribution throughout a cell is then taken as being a combination of a uniform background resulting from naturally occurring dose, and sharp spikes, which are the result of the addition of GNPs. The number of GNP ionizations-and thus dose spikes- per cell can be calculated by multiplying the number of ionizations in a single nanoparticle per Grey by the number of GNP per cell and the prescribed dose. Each ionization is then assumed to deposit a dose distribution around it as calculated by the nanodosimetry model. These ionizing events are then added to the uniform background with a random distribution, based on the

assumption of a sparse, uniform distribution of GNPs. This then gives a distribution of dose throughout the cell on the nanoscale, taking into account inhomogeneities introduced by the GNPs, which can be used as input to the LEM. (McMahon S. , et al., 2011)

If we analyze the variation in dose near the nanoparticle in nanoscale distances, we will see doses of the order of thousands of Gy deposited in the vicinity of the nanoparticle following a single ionizing event. The combination of extremely high doses and extremely small volumes is relatively uncommon in x-ray radiotherapy, as the incident radiation is typically very sparsely ionizing. Distributions of this sort are regularly seen around particle tracks in charged particle therapies. The hypothesis that the high degree of dose localization near GNPs is responsible for the large dose enhancements observed experimentally was tested by applying a predictive framework which has been successful in accounting for the biological effects of dose inhomogeneity in heavy ion therapy. To quantify this effect, the Local Effect Model (LEM) has been applied to the inhomogeneous dose distributions around GNPs to determine what additional cell killing results from this effect.

The predictions of the LEM are closely related to the cell line under consideration. Taking into account the dose inhomogeneity in the vicinity of GNPs using the LEM leads to predicted RBEs which are several times greater than those predicted by the change in macroscopic dose alone. This increase in effectiveness is in qualitative agreement with experimental results, suggesting that these dose inhomogeneities may be responsible for some or all the large enhancements which are observed experimentally.

Unfortunately the connection between the obtained results of dose deposition by MC simulation and the results that the authors present of the cell survival curves are not clearly presented. The authors assure that by combining the nanoscale dose distribution and ionization rates for the amount of gold within a cell and the cell line's fitted with α and β parameters in the absence of gold, predictions of the radiosensitizing effect of GNPs can be obtained using the LEM. This allows for predictions to be made about α and β parameters in the presence of GNPs at each energy, and thus the degree of radiosensitization achieved through the addition of GNPs, without reference to the experimental observed results.

After calculations the corresponding curves obtained as dashed lines are presented in Figure 1.6. It can be see that these curves are in good agreement with the observed radiation response

of GNPs, closely following the experimental measured points. Values obtained for the α and β parameters are in good agreement with the measured from the experimental results. The lack of description of how they obtain those values is a limiting factor when we try to reproduce it.
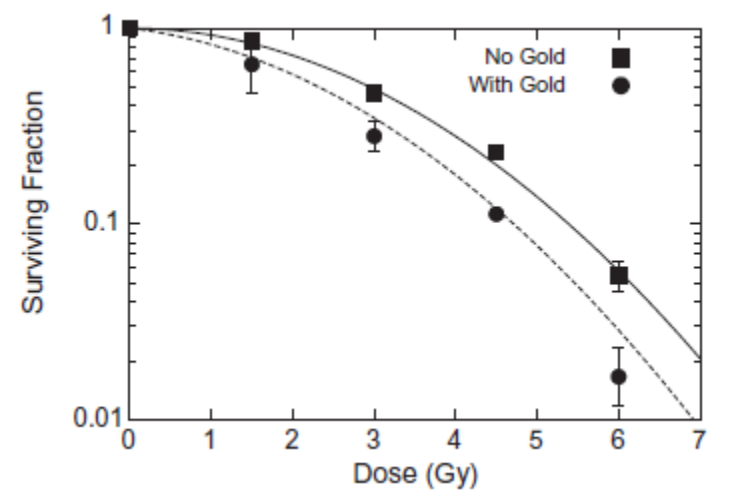

Figure 1.6 Comparison of LEM predictions and observed experimental results for MDA-MB-231 cells exposed to   MV radiation, with and without GNPs.   Points are measured values (squares, control; diamonds, with gold). The solid line is a fit to the control cell response curve, while the dashed line is the LEM prediction for the radiation response in the presence of GNPs. Adapted from (McMahon, 2011)

The dominance of short-range effects highlights the importance of the sub-cellular uptake and localization. The observed dose enhancement varies significantly between different cell lines, suggesting that enhancement depends significantly on the biological distribution of the GNPs within the cell. These observations highlight the importance of improved understanding of sub-cellular localization of the contrast agents, as agents which see and inhomogeneous distribution may see a decreased efficacy, as GNPs which are localized far from sensitive areas within the cell would be less likely to lead to cell death.

A relatively small number of well-targeted particles could potentially lead to a significant concentration within the cell nucleus, and correspondingly large RBE. Additionally, the relative inactivity of the core of the nanoparticle is of potential to approaches which seek to optimize nanoparticle properties by combining cores and coatings of different materials.

CHAPTER II. GENERAL EQUATIONS DESCRIBING NANOSCALE DOSE DISTRIBUTION IN CRITICAL STRUCTURES WITH EMBEDDED GOLD NANOPARTICLES.

The global aim of theoretical consideration of GNP-aided radiation therapy is the estimation of survival of GNP loaded tumor cells irradiated with external (Linac, X-ray tube) and internal (brachytherapy) photon sources. Four almost independent stages should be described to quantify the cell survival after irradiation (Zygmanski, et al., 2013). The first stage simulates the photon transport across macroscopic depths from a clinical radiation source to a tumor region and relates the spectral characteristics of the incident beam to the radiation fluence at the tumor cell location. In the second stage, this fluence is used as the radiation source for new simulations that allow to describe the interaction of fluence with GNPs and to calculate the radial dose distribution around single or multiple GNPs. The third stage describes the dose distribution in a cell structures linking the radial dose distribution for individual GNPs and the GNP distribution in the cell. The last, forth stage relates the cell survival probability to the dose distribution in cell structures loaded with GNPs.

In the following, we will present a set of general expressions describing the second, third and fourth stages that constitute an analytical framework for the assessment of cell survival in GNP radiotherapy. The first stage simulates the photon transport across macroscopic depths in a homogenous medium ignoring the nanoscale heterogeneity caused by the presence of GNPs. This stage is typically provided with macroscopic Monte Carlo simulations and is excluded from our analytical framework. But the simulated at this stage radiation fluence will be included in the framework as an input variable. We also will ignore the complex structure of biological cells and will suppose that GNPs are embedded in pure water.

2.1 PHOTON INTERACTION WITH A GNP AND THE CREATION OF SECONDARY ELECTRONS

Let's consider a single GNP embedded in a homogenous medium (water) under photon irradiation. As was mentioned above, the fluence at the location of cell should be found by MC simulations and will be considered here as an input variable. Moreover, we will suppose that the photon fluence is homogenous and isotropic within the cell:

$$\Phi = \int_0^\infty \Phi_E(E_{ph}) dE_{ph} \qquad (2.1)$$

where $\Phi_E(E_{ph})$ is the normalized energy distribution of the fluence (normalized incident photon spectrum).

The mean number of photon interaction per target entity in a certain small volume subjected to incident photons with energies between E_{ph} and $E_{ph} + dE_{ph}$ can be found from the definition of the cross section is (ICRU85, 2011)

$$dN_{int}(E_{ph}) = \sigma(E_{ph})\Phi_E(E_{ph}) dE_{ph} \quad (2.2)$$

Taking into account the relation between the total cross section and the mass attenuation coefficient (ICRU85, 2011) we can write

$$\frac{dN_{int}(E_{ph})}{dE_{ph}} = \sigma_{tot}(E_{ph})\Phi_E(E_{ph}) = \frac{M}{A_0}\frac{\mu(E_{ph})}{\rho}\Phi_E(E_{ph}) \quad (2.3)$$

the quantity M in Eq.(2.3) is the molar mass of the target entity material. If the target entity is gold ($M_{Au} = 196.97\ g$) and $A_0 = 6.022x10^{23}$ is the Avogadro's constant. The equation

$$N_{int,Au} = \frac{M_{Au}}{A_0}\int_0^\infty \left[\frac{\mu(E_{ph})}{\rho}\right]_{Au} \Phi_E(E_{ph}) dE_{ph} \quad (2.4)$$

gives the mean number of photon interactions per gold atom.

The mean number of photon interactions per GNP is proportional to the photon fluence Φ. To find the coefficient of proportionality one should replace M_{Au} with $M_{GNP} = V_{GNP}\rho_{Au}A_0$ and extract the fluence (which is energy independent) from the integral (2.4)

$$N_{int,GNP} = \rho_{Au}V_{GNP}\Phi\int_0^\infty \left[\frac{\mu(E_{ph})}{\rho}\right]_{Au} \frac{\Phi_E(E_{ph})}{\Phi} dE_{ph} \quad (2.5)$$

here $V_{GNP} = \frac{4\pi}{3}R_{NP}^3$ is the GNP volume and $\Phi_E(E_{ph})/\Phi$ is the energy distribution of the fluence described by Eq(2.1).

The expression (2.5) is valid for any GNP shape. It only assumes that the attenuation of the photon beam is negligible over the GNP size, and every point in the GNP experiences the same photon fluence.

Direct comparison of the mass attenuation coefficients for tissue and gold shows that the photoelectric effect is the principal interaction mode at photon energy less than 300 keV. Its probability is determined by the ratio $k_{pe}(E_{ph})$. In the photoelectric interaction between a photon of energy E_{ph} and an atom the photoelectron is ejected from the atom with a kinetic energy

$$E_e = E_{ph} - E_j \quad (2.6)$$

leaving behind a vacancy in the shell or subshell from which it was ejected. The energy E_j is the binding energy of the $j-shell$ or $j-subshell$ electron (where j stands for the K shell, three L subshells, five M subshells and so on). The number of interactions with the specific subshell is determined by the probability $P_j(E_{ph})$, which is the probability for the photoelectric effect, if it occurs, to occur in the j subshell of an absorber atom. The photon energy E_{ph} must exceed the threshold energy E_j for the photoelectric event to occur in subshell j. Taking into account that the energy of a secondary photoelectron is determined by incident photon energy through Eq. (2.6) and that each photon interaction creates a secondary electron, the number of electrons ejected from GNP with energy E_e (the energy spectrum of the secondary photoelectrons created in the GNP) can be written as

$$\frac{dN_{pe,GNP}(E_e)}{dE_e} = \rho_{Au} V_{GNP} \Phi \sum_j k_{pe}(E_e + E_j) P_j(E_e + E_j) \left[\frac{\mu(E_e + E_j)}{\rho}\right]_{Au} \frac{\Phi_E(E_e + E_j)}{\Phi} \quad (2.7)$$

The atomic relaxation of ionized subshells results in emission of the characteristic X-ray fluorescence and Auger electrons. The number of characteristic photons (sometimes called fluorescent photons) emitted per orbital electron vacancy in subshell j is referred to as fluorescent yield ω_j, while the number of Auger electrons emitted per orbital electron vacancy is equal to $(1 - \omega_j)$. The fluorescent yield depends on the atomic number Z of the atom and on the principal quantum number of a shell.

The characteristic X-rays are absorbed sufficiently far from the GNP, do not significantly contribute to the dose around a GNP and will not considered here. From the other hand, low energy Auger electrons are absorbed in and near the GNP and provide significant and often major contribution to the dose deposition near the GNP surface.

In the Auger process the ionized subshell, of binding energy E_j, is filled by an electron from an outer subshell, of binding energy E_i, and the excess energy $(E_j - E_i)$ is given to another electron in a still more shallow one of binding energy E_h. The kinetic energy E_{jih} of the ejected Auger electron, is then

$$E_{jih} = E_j - E_i - E_h \quad (2.8)$$

in contrast to photoelectron, the energy of the Auger electron does not depend on the energy of the incident photon.

Multiplication Eq. (2.5) with $P_j(E_{ph})$, and the Auger electrons yield, $(1 - \omega_j)$ and integration over the energy higher the E_j give the total number the Auger cascades, $N_{PA,j,GNP}$ initiated by the creation of the initial vacancy in the subshell j

$$N_{pA,j,GNP} = \rho_{Au} V_{GNP} (1 - \omega_j) \Phi \int_{E_j}^{\infty} k_{pe} (E_e + E_j) P_j (E_{ph}) \left[\frac{\mu(E_{ph})}{\rho} \right]_{Au} \frac{\Phi_E(E_{ph})}{\Phi} dE_{ph} \quad (2.9)$$

The discrete spectrum of the Auger electrons created in a GNP after interaction of incident photons with the energy distribution of fluence $\Phi_E(E_{ph})$ can be presented as a sum

$$\frac{dN_{PA,GNP}(E_e)}{dE_e} = \sum_j N_{PA,j,GNP} \sum_i \sum_h A_{jih} \delta(E_e - E_j + E_i + E_h) \quad (2.10)$$

where coefficients A_{jih} are the number of Auger electrons with he kinetic energy E_{jih} after the creation of initial vacancy in the subshell j.

2.2 THE DOSE DELIVERED BY ONE ESCAPED SECONDARY ELECTRON IN THE VICINITY OF A GNP.

After interaction of incident photons with a GNP a number of secondary electrons of various energies are created. Below we present equations describing the dose delivered by one escaped secondary electrons created in an irradiated GNP.

Let's suppose that an incident photon creates in a certain point of GNP one electron of energy E_0. In fact, the photon does not create electron, only knock out it from a gold atom, therefore the terms "creation of secondary electrons" and similar are formally incorrect. However, we will use this term because of its convenience and simplicity.

Geometry assumed for estimation of energy deposition by electrons created in NP is shown in Figure 2.1 (Chernov, Chernov, & Barboza-Flores, 2012). A spherical GNP of radius R_{NP} is centered at the origin O of a spherical coordinate system (in the figure the radius of the GNP is presented as a_0). An electron is created at a point A_0 at distance l from the NP surface. At a point A_1 the electron crosses the GNP surface and travels at the angle α relative to the normal of the GNP surface at the point A_1, continuing to travel in the surrounding medium. At a point A_2 the electron reaches a sphere of radius r centered on the center of the GNP.
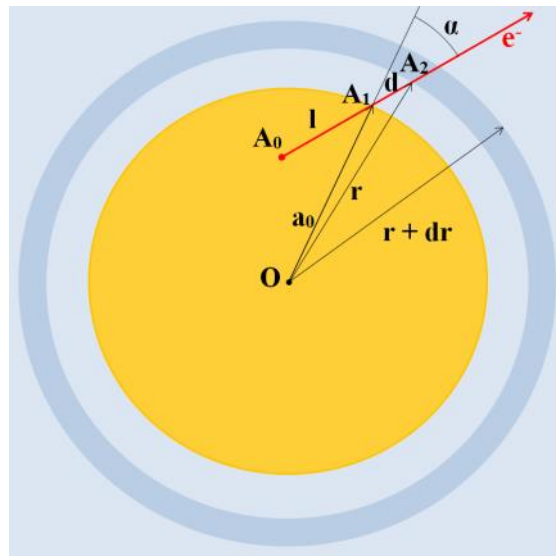

Figure 2.1 Geometry assumed for the estimation of the energy deposition by electrons created in GNP.

During travel, the electron losses energy and slows down. If its energy is sufficiently high, the electron crosses the GNP surface, continues to travel in the medium and eventually stops. In our calculations, we will use the continuous slowing down approximation (CSDA). In this approximation, the rate of energy loss is assumed to be equal to the total stopping power and energy-loss fluctuations are neglected (ESTAR, 2012) .

The rest electron energy at the NP surface E_1 and the electron energy at distance r from the GNP center $E_2(r)$ are determined by its initial energy E_0 and distances l and d that the electron passes in the GNP and in a cell (the lengths A_0A_1 and A_1A_2 in Figure2.1, respectively. Assuming that emitted electrons travel in a straight-line path, the energies can be found from the equations

$$R_p(E_1) = R_p(E_o) - l$$

$$R_m(E_2(r)) = R_m(E_1) - d \qquad (2.11)$$

where the functions $R_{Au}(E)$ and $R_w(E)$ are the electron range - energy relationships for gold and water (the main cell constituent) that relate a residual range and an electron energy. The distance d is equal to

$$d = \sqrt{r^2 - R_{NP}^2 sin^2\alpha} - R_{NP}cos\alpha \quad (2.12)$$

where α is the angle at which an electron escapes the GNP (relative to the normal of the GNP surface). Inversion the first part of (2.11) with respect to E_1 and the second one with respect to E_2 gives

$$E_1(E_0, l) = R_{Au}^{-1}[R_{Au}(E_0) - l],$$

$$E_2(r, E_0, l, \alpha) = R_w^{-1}\left\{R_w[E_1(E_0, l)] - \sqrt{r^2 - R_{NP}^2 \sin^2\alpha} + R_{NP}\cos\alpha\right\}$$

$$(2.13)$$

where the inverse functions $R_{Au}^{-1}(R)$ and $R_W^{-1}(R)$ are the energies of electron with given range R in gold and water, respectively.

To find the average energy of escaped electrons at the distance r from the GNP center, $Eav(E_0, l)$ Eq. (2.13) should be integrated over all possible travel distances in the GNP l and the escaping angles α

$$E_{av}(E_0, r) = \iint\limits_{E_2(r, E_0, l, \alpha) > 0} \psi(l, \alpha) E_2(r, E_0, l, \alpha) dl d\alpha$$

(2.14)

here $\psi(l, \alpha) dl d\alpha$ is the probability that the created electron in the GNP has passed the distance between l and $l + dl$ in the GNP and left the GNP at an angle between α and $\alpha + d\alpha$ relative to the normal of the GNP surface at the point of escaping. The integral (2.14) is taken over those l and α, for which $E_2(r, E_0, l, \alpha) > 0$.

The function $\psi(l, \alpha)$ depends on the distribution of the created electrons over the GNP volume and their directions of travel. In the case of the homogenous and isotropic creation of secondary electrons and straight-line electron traveling, the function $\psi(l, \alpha)$ can be found from a geometrical consideration, similar to that used in the MIRD formalism to estimate the absorbed dose at the cellular level from intracellularly localized radionuclides (Goddu, Howell, & Rao, 1994) (Chernov, Chernov, & Barboza-Flores, 2012)

$$\psi(l, \alpha) = \frac{3 \sin \alpha \cos \alpha}{2 R_{NP}}$$

(2.15)

The values of l and α are limited by the conditions

$$0 \leq l \leq 2R_{NP}; 0 \leq \alpha \leq \alpha_{max} = \cos^{-1}(l/2R_{NP})$$

(2.16)

The dose delivered at a distance r from the GNP center or the radial dose distribution, $D(r)$, is defined as the average energy deposited in a spherical shell with the radii between r and $r + dr$, normalized to its mass

$$D(r) = -\frac{dE_{av}(r)}{4\pi r^2 \rho_w dr}$$

(2.17)

where ρ_w is the surrounding medium (water) density. The minus sign comes from the fact that $E_{av}(r)$ always decreases when r increases.

The set of equations (2.11) – (2.17) allows to find the radial dose distribution (RDD) around a GNP per one created electron with energy E_0. If photon irradiation creates electrons of various energies, the equations should be averaged over a spectrum of the secondary electrons. An analytical expressions describing RDD can be derived in the case of the simplest supposition that the residual range of electron is proportional to its energy (Chernov G. , 2014). Several cases depending on relationships between various parameters of length dimension could be considered. The most important for this thesis case corresponds to RDD in vicinity of a sufficiently small GNP. A GNP will be considered as small if the range of the created electron of energy E_0 in gold, R_{Au} is greater than the GNP diameter ($2R_{NP} < R_{\mathrm{Au}}$). The vicinity of the GNP considered is determined by the condition

$$\mathrm{R}_{NP} \leq r \leq \mathrm{R}_{NP} + \left(R_{Au} - 2\mathrm{R}_{NP} \right) \frac{R_w}{R_{Au}} \quad (2.18)$$

where R_w is the range of electron of energy E_0 in water.

The RDD for this case is described by expression

$$D(r) = \frac{3E_0}{4\pi R_{NP}^2 \rho_w R_w} \left[\frac{1}{2} + \frac{\left(r^2 - R_{NP}^2 \right)}{4R_{NP}r} \ln\left(\frac{r - R_{NP}}{r + R_{NP}} \right) \right] \quad (2.19)$$

2.3. THE RELATION BETWEEN THE DOSES DELIVERED BY SECONDARY ELECTRONS ESCAPING FROM A GNP AND IN SURROUNDING WATER.

Eq. (2.19) describes the RDD per one created photoelectron (or one photon interaction with gold atom) in a GNP. For practical applications, it is needed to relate the dose delivered by escaping secondary electrons to the dose in water in vicinity of the X-ray irradiated GNP and a number of created electrons. The given photon fluence Φ with the energy distribution $\Phi_E(E)$ interacts with a GNP and knock out a number of secondary photoelectrons Eq. (2.5) and Auger electrons Eq. (2.9). The given photon fluence will interact with water delivering a dose D_w in the vicinity of the GNP. In the case of charged-particle equilibrium the kerma serve as approximations to absorbed dose, then the absorbed dose in water can be written as (ICRU85, 2011)

$$D_w = \Phi \int_0^\infty E_{ph} \left[\frac{\mu_{tr}(E_{ph})}{\rho} \right]_w \frac{\Phi_E(E_{ph})}{\Phi} dE_{ph} \qquad (2.20)$$

where $(\mu_{tr}/\rho)_w$ is a mass energy-transfer coefficient of water.

It follows from Eq. 2.20 that

$$\Phi = \frac{D_w}{\int_0^\infty E_{ph} \left[\frac{\mu_{tr}(E_{ph})}{\rho} \right]_w \frac{\Phi_E(E_{ph})}{\Phi} dE_{ph}} \qquad (2.21)$$

The substitution of Eq. 2.21 into Eq.2.7 give us the relationship between the spectrum of created photoelectrons in the spherical GNP of radius R_{NP} and the dose in surrounding water (sufficiently far from the GNP), D_w.

$$\frac{dN_{pe,GNP}(E_e)}{dE_e} = \frac{4\pi a_0^3 \rho_{Au} \sum_j k_{pe}(E_e + E_j) P_j(E_e + E_j) \left[\frac{\mu(E_e + E_j)}{\rho} \right]_{Au} \frac{\Phi_E(E_e + E_j)}{\Phi}}{3 \int_0^\infty E_{ph} \left[\frac{\mu_{tr}(E_{ph})}{\rho} \right]_w \frac{\Phi_E(E_{ph})}{\Phi} dE_{ph}} D_w \quad (2.22)$$

Integrating the dose per one created photoelectron of energy E_e (Eq. 2.19) over their spectrum Eq. 2.22 from 0 to the maximal energy of photoelectrons, E_{max}, gives us the relationship between the dose delivered in a vicinity of the GNP and dose in surrounding water

$$\begin{aligned}
D_{pe}(r) &= \int_0^{E_{max}} \frac{3E_e}{4\pi a_0^2 \rho_w R_w(E_e)} \left[\frac{1}{2} + \frac{(r^2 - a_0^2)}{4a_0 r} \ln\left(\frac{r - a_0}{r + a_0} \right) \right] \frac{dN_{pe,GNP}(E_e)}{dE_e} dE_e = \\
&= \frac{a_0 \rho_{Au} C_\mu}{\rho_w} \left[\frac{1}{2} + \frac{(r^2 - a_0^2)}{4a_0 r} \ln\left(\frac{r - a_0}{r + a_0} \right) \right] D_w
\end{aligned} \qquad (2.23)$$

where

$$C_\mu = \frac{\int_0^{E_{max}} \sum_j k_{pe}(E_e + E_j) P_j(E_e + E_j) \left[\frac{\mu(E_e + E_j)}{\rho} \right]_{Au} \frac{\Phi_E(E_e + E_j)}{\Phi} \frac{E_e}{R_w(E_e)} dE_e}{\int_0^\infty E_{ph} \left[\frac{\mu_{tr}(E_{ph})}{\rho} \right]_w \frac{\Phi_E(E_{ph})}{\Phi} dE_{ph}} \qquad (2.24)$$

The coefficient C_μ does not depend on the GNP radius and it is determined by the parameters describing the interaction of photons with water and gold. For the case of the monoenergetic photon fluence, $\Phi_E(E_{ph}) = \delta(E_{ph} - E_{ph0})$, $E_e + E_j = E_{ph0}$ and Eq. 2.24 can be presented as

$$C_\mu(E_{ph}) = \frac{\left[\dfrac{\mu(E_{ph0})}{\rho}\right]_{Au}}{\left[\dfrac{\mu_{tr}(E_{ph0})}{\rho}\right]_w} \frac{k_{pe}(E_{ph0})\sum_j P_j(E_{ph0})\dfrac{E_{ph0} - E_j}{R_w(E_{ph0} - E_j)}}{E_{ph0}} \quad (2.25)$$

if the photon energy is higher than $E_K = 80.7\ keV$, photons will mainly interact with K shell electrons, therefore

$$C_\mu(E_{ph}) = k_{pe}(E_{ph0})P_j(E_{ph0})\frac{E_{e0}}{R_w(E_{e0})E_{ph0}}\left(\left[\frac{\mu(E_{ph0})}{\rho}\right]_{Au} \Big/ \left[\frac{\mu_{tr}(E_{ph0})}{\rho}\right]_w\right) \quad (2.26)$$

where $E_{e0} = E_{ph0} - E_k$ is the initial energy of photoelectron ejected from a gold atom.

2.4 THE ENERGY DELIVERED IN A SPHERICAL CRITICAL CELL STRUCTURE BY ONE GNP.

In the following, we will derive an expressions describing the dose distribution $p(D)$ in a critical structure an X-ray irradiated cell with one embedded GNP. For simplicity, the critical structure and GNP be considered as spheres of radii R_{st} and R_{NP}, respectively. We will suppose that the RDD is spherically symmetric and described by a decreasing function D(r), where r is the distance from the GNP center. Depending on a distance L between the critical structure and the GNP two cases should be considered: the GNP is located inside or outside of the critical structure.

The dose distribution function $p(D)dD$ describes the distribution of dose within the critical structure. It is defined as the volume with doses between D and $D + dD$ normalized on the structure volume V_{st}

$$p(D)dD = \frac{1}{V_{st}} \int_{D \leq D(r) \leq D + dD} d^3\vec{r} \quad (2.27)$$

or

$$p(D) = \frac{1}{V_{st}} \int_{V_{st}} \delta[D - D(\vec{r})] d^3\vec{r} \quad (2.28)$$

where $D(\vec{r})$ is the spatial dose distribution within the structure and the three-dimensional integral is taking over the structure volume V_{st}.

2.4.1 The GNP is located outside of the critical structure.

In the case of $L > R_{st} + R_{NP}$ the GNP is located outside of the critical structure. The sketch presenting this case is shown in Figure 2.2. The GNP is centered at the origin O of a spherical coordinate system. The polar angle θ is measured from the z–axis that passes through the critical structure center O_1. The surface at a current distance r on which the dose has the constant value $D(r)$ is shown by the dash line. The polar angle at which this surface crosses the structure surface is denoted as θ_{max}.
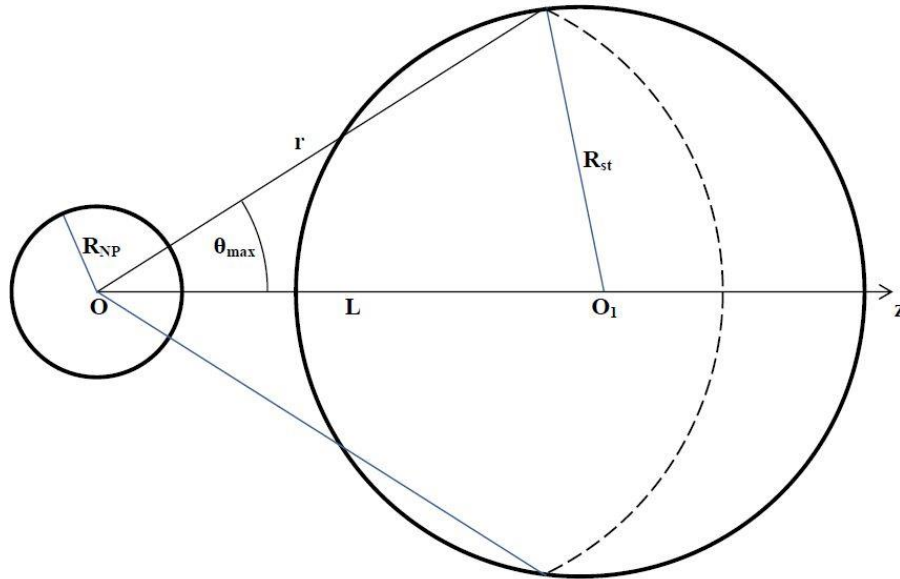

Figure 2.2 Geometry assumed for the description of the case 1, when the GNP is located outside of the critical structure (cell) (see explanation in the text).

Because of simple geometry the integral (2.28) can be easily reduced to an iterated integral with the integration over the spherical coordinates r, θ and φ

$$p(D) = \frac{1}{V_{st}} \int_{R_{min}}^{R_{max}} dr r^2 \delta[D - D(r)] \int_{0}^{\theta_{max}(r)} d\theta \sin\theta \int_{0}^{2\pi} d\varphi \quad (2.29)$$

where $R_{min} = L - R_{st}$ and $R_{max} = L + R_{st}$ are closest and the farthest distances from the GNP center to the surface of the structure, respectively.

The integration over φ gives 2π. Taking into account that $d\theta \sin\theta = -d(\cos\theta)$ and

$$V_{st} = \frac{4\pi}{3} R_{st}^3 \quad (2.30)$$

we can rewrite Eq.(2.29) as

$$p(D) = \frac{3}{2R_{st}^3} \int_{R_{min}}^{R_{max}} dr \, r^2 \delta[D - D(r)] \int_{\cos\theta_{max}(r)}^{1} d(\cos\theta)$$

$$(2.31)$$

or

$$p(D) = \frac{3}{2R_{st}^3} \int_{R_{min}}^{R_{max}} dr \, r^2 \delta[D - D(r)] \, [1 - \cos\theta_{max}(r)]$$

$$(2.32)$$

The angle θ_{max} is a function of the current radius r in the target sphere. The dependence of θ_{max} on r can be found with the cosine theorem

$$\cos \theta_{max} = \frac{r^2 + L^2 - R_{st}^2}{2rL} \quad (2.33)$$

Substituting Eq.(2.33) in Eq.(2.32) we will have

$$p(D) = \frac{3}{2R_{st}^3} \int_{R_{min}}^{R_{max}} dr \, r^2 \delta[D - D(r)] \left(1 - \frac{r^2 + L^2 - R_{st}^2}{2rL} \right)$$

$$(2.34)$$

or

$$p(D) = \frac{3}{4R_{st}^3 L} \int_{R_{min}}^{R_{max}} dr \, r \delta[D - D(r)] \, (R_{st} + L - r) \, (R_{st} - L + r)$$

$$(2.35)$$

The radial dose distribution $D(r)$ is monotonic single-valued decreasing function. Therefore we can express the current radius r as a function of dose, $r(D)$ and pass from integration over r to integration over D

$$p(D) = \frac{3}{4R_{st}^3 L} \int_{D_{min}}^{D_{max}} dD_1 \left[-\frac{dr(D_1)}{dD_1} \right] r(D_1)[R_{st} + L - r(D_1)] \, [R_{st} - L + r(D_1)] \, \delta[D - D_1]$$

(2.36)

where $D_{min} = D(L + R_{st})$ and $D_{max} = D(L - R_{st})$, respectively. The presence of the delta function allows taking integral (2.36) for any integrand that gives:

$$p(D) = 0, \quad 0 \le D \le D_{min}$$

$$p(D) = \frac{3r(D)[R_{st} + L + r(D)] \, [R_{st} - L + r(D)]}{4R_{st}^3 L} \left[-\frac{dr(D)}{dD} \right], D_{min} \le D \le D_{max}$$

$$p(D) = 0, \quad D \ge D_{max}$$

(2.37)

2.4.2 The GNP is located inside of the critical structure.

In the case of $L < R_{st} - R_{NP}$ the GNP is located inside of the critical structure. The sketch presenting this case is shown in Figure 2.3. The symbols and their meaning are the same of Figure 2.2.

As in the previous case, the simple spherical geometry allows to reduce the three-dimensional integral (2.28) to the iterated integral (2.29). Only integration limits should be changed. It is easy to see in Figure 2.3 that for $R_{NP} < r < R_{st} - L$ the angle θ_{max} will be equal to π and the integral (2.29) should be rewritten as

$$p(D) = \frac{3}{2R_{st}^3} \left\{ \int_{R_{NP}}^{R_{st}-L} dr \, r^2 \delta[D - D(r)] \int_{-1}^{1} d(cos\theta) \right.$$
$$\left. + \int_{R_{st}-L}^{R_{st}+L} dr \, r^2 \delta[D - D(r)] \int_{cos\theta_{max}(r)}^{1} d(cos\theta) \right\}$$
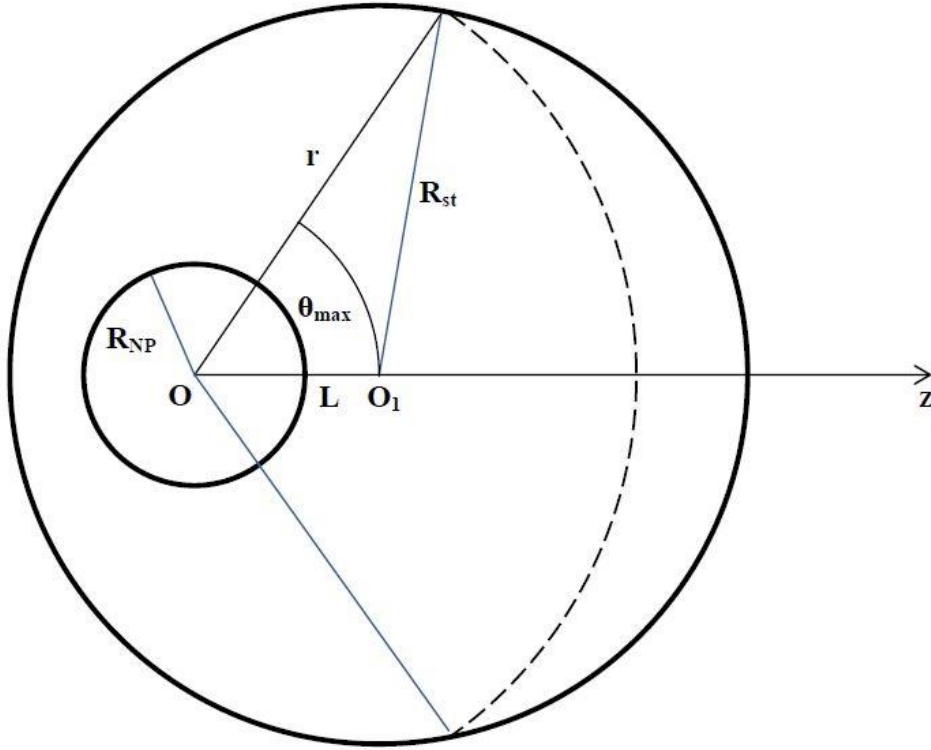
(2.38)

44

Figure 2.3 Geometry assumed for the description of the second case, when the GNP is located inside of the critical structure (see explanation in the text).

or

$$p(D) = \frac{3}{2R_{st}^3}\left\{2\int_{R_{NP}}^{R_{st}-L} dr\, r^2\delta[D - D(r)] + \int_{R_{st}-L}^{R_{st}+L} dr\, r^2\delta[D - D(r)][1 - cos\theta_{max}(r)]\right\}$$

(2.39)

The dependence of θ_{max} on r is the same as for the first case Eq.(2.33), therefore we can omit the steps describing by Eqs.(2.33)-(2.35) and present the dose distribution as:

$$p(D) = 0, \quad 0 \le D \le D_{min}$$

$$p(D) = \frac{3r(D)[R_{st} + L - r(D)]\,[R_{st} - L + r(D)]}{4R_{st}^3 L}\left[-\frac{dr(D)}{dD}\right], D_{min} \le D \le D_{max}$$

$$p(D) = \frac{3r^2(D)}{R_{st}^3}\left[-\frac{dr(D)}{dD}\right] D_{max} \leq D \leq D_{NP}$$

$$p(D) = 0, \quad D \geq D_{NP}$$

$$(2.40)$$

where $D_{min} = D(R_{st} + L)$, $D_{max} = D(R_{st} - L)$ and $D_{NP} = D(R_{NP})$, respectively.

2.5 THE ENERGY DELIVERED IN A SPHERICAL CRITICAL CELL STRUCTURE BY SEVERAL GNPS.

The function describing the dose distribution within a critical structure from several GNPs located inside or/and outside its volume can be presented as

$$p(D) = \frac{1}{V_{st}} \int_{V_{st}} \delta\left[D - \sum_{i=1}^{N} D_i(\vec{r})\right] d^3\vec{r} \quad (2.41)$$

where N is the number of GNPs and

$$D_i(\vec{r}) = D(|\vec{r} - \vec{r}_i|) \quad (2.42)$$

is the RDD from a GNP located at the position $\vec{r}_i$ in the coordinate system related to the critical structure.

It should be note that Eq.(2.42) corresponds only to the dose delivered by secondary electrons escaped from gold atoms. The dose delivered by secondary electrons from water will assumed to be constant and equal to D_w.

In fact, the integral (2.41) is too complex to be taken analytically for an arbitrary set of GNP positions and could be evaluated numerically. MC simulations and analytical considerations of RDD clearly indicate that dose gradually decreases with increasing the distance from the GNP center. This means that at distances sufficiently far from the GNP center the dose delivered by secondary electron escaped from the GNP will be much lower than dose in water D_w. Then we can introduce a critical radius R_c at which the dose related to a GNP is

sufficiently small to compare with D_w and corresponding to this radius the critical volume V_c

$$D(R_c) = k_c D_w << D_w \quad (2.43)$$

$$V_c = \frac{4\pi}{3} R_c^3 \quad (2.44)$$

where k_c is the coefficient (equal, for instance 0.1) specifying (quantifying) the condition $D(R_c) << D_w$.

Let's assume that all GNPs are located inside the structure, they are identical, their number in the structure is sufficiently small, the distances between the GNP centers more than $2R_c$ and the distances from the GNP centers to the structure surface more than R_c. In this case, we can divide the structure volume in two parts. The first volume, $V_1 = NV_c$, consists of N nonoverlapping spheres of radius R_c with the same dose distribution $p1(D)$ among them (grey regions). The second volume, $V_2 = V_{st} - V_1$, is the volume between the nonoverlapping spheres Figure 2.4. With the above assumptions, Eq. (2.34) can be rewritten as

$$p(D) = \frac{1}{V_{st}} \int_{\vec{r} \in V_2} \delta(D - D_w) d^3\vec{r} + \frac{1}{V_{st}} \sum_{i=1}^{N} \int_{|\vec{r} - \vec{r}_i| \leq R_c} \delta[D - D(|\vec{r} - \vec{r}_i|) - D_w] d^3\vec{r} \quad (2.45)$$

All GNPs were assumed to be identical and their centers are located at larger distances than R_c from the structure surface, therefore, the terms under summation are all the same (all r_i can be replaced by 0) and

$$p(D) = \frac{\delta(D - D_w)}{V_{st}} \int_{\vec{r} \in V_2} d^3\vec{r} + \frac{N}{V_{st}} \int_{|\vec{r}| \leq R_c} \delta[D - D(|\vec{r}|) - D_w] d^3\vec{r} \quad (2.46)$$

After integration

$$p(D) = \left(1 - \frac{V_c}{V_{st}}\right) \delta(D - D_w), \quad 0 < D \leq D_w$$
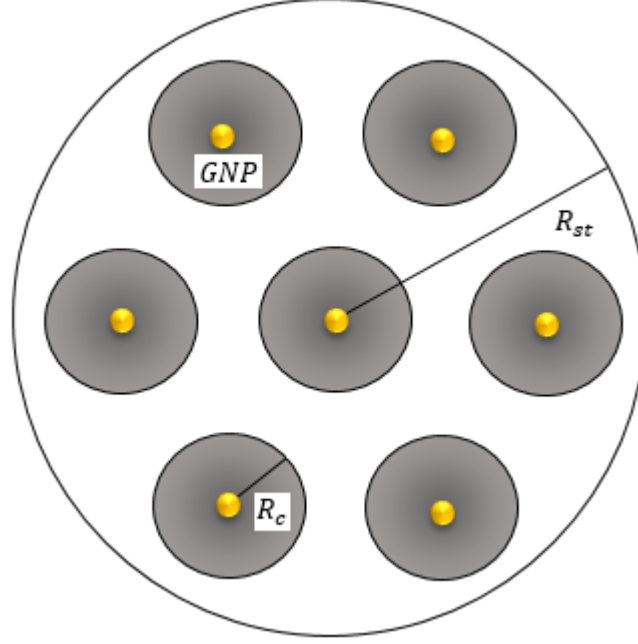$$p(D) = Np_1(D), \quad D > D_w \quad (2.47)$$

Figure 2.4 Schematic representation of the target structure with embedded gold nanoparticles, the critical radius R_c around the GNPs defines the regions where the dose deposition is not negligible when compare with the prescribed dose D_w.

where

$$p_1(D) = \frac{4\pi}{V_{st}} \int_0^{R_{NP}} \delta(D) r^2 dr + \frac{4\pi}{V_{st}} \int_{R_{NP}}^{R_c} \delta[D - D(r) - D_w] r^2 dr \quad (2.48)$$

The second integral in Eq.(2.48) can be taken as integral (2.36)

$$p_1(D) = \frac{3}{R_{st}^3} \int_{D_w + D(R_c)}^{D_w + D(R_{NP})} dD_1 \left[-\frac{dr(D_1 - D_w)}{dD_1} \right] r^2(D_1 - D_w) \delta(D - D_1),$$

$$p_1(D) = \frac{3}{R_{st}^3} \left[-\frac{dr(D - D_w)}{dD} \right] r^2(D - D_w), \quad D_w + D(R_c) \le D \le D_w + D(R_{NP}) \quad (2.49)$$

CHAPTER III. DOSE DISTRIBUTION IN A SPHERICAL CRITICAL CELL STRUCTURE: $1/r^2$ RADIAL DOSE DISTRIBUTION DEPENDENCE.

3.1. RADIAL DOSE DISTRIBUTION AROUND A GNP PER ONE CREATED PHOTOELECTRON; THE CASE OF $1/r^2$ DEPENDENCE

Recalling Eq.(2.19); the radial dose distribution around the GNP is defined by

$$D(r) = \frac{3E_0}{4\pi R_{NP}^2 \rho_w R_w} \left[\frac{1}{2} + \frac{(r^2 - R_{NP}^2)}{4R_{NP}r} \ln\left(\frac{r - R_{NP}}{r + R_{NP}}\right) \right] \quad (2.19)$$

where E_0 is the kinetic energy of the photoelectron with which they leaves the GNP surface, R_{NP} is the GNP radius, ρ_w is the density of the media surrounding the GNP (water in this case), R_w is the range of the photoelectron in the media and r is the current distance measured from GNP center where the dose deposition is being measured. The equation (33) is only valid for radius

$$r \leq R_{NP} + R_w \left(1 - \frac{2R_{NP}}{R_{Au}}\right) \quad (3.1)$$

For a small GNP when $R_{NP} \ll R_{Au}$ the condition (3.1) is valid at distances sufficiently far from a GNP (where R_{Au} is the photoelectron range in the nanoparticle media (gold)). Introducing a small parameter $t = R_{NP}/r$ we can rewrite Eq.(2.23) as

$$D_1(r) = \frac{3E_0}{4\pi R_{NP}^3 \rho_w} \frac{R_{NP}}{R_w} \left[\frac{1}{2} + \frac{1}{4}\left(\frac{1}{t} - t\right) ln\left(\frac{1-t}{1+t}\right)\right]$$

$$(3.2)$$

The Taylor series expansion of the expression in squared brackets around $t = 0$ gives (the odd terms are equal to 0)

$$D_1(r) = \frac{3E_0}{4\pi R_{NP}^3 \rho_w} \frac{R_{NP}}{R_w} \left[\frac{t^2}{3} + \frac{t^4}{15} + \frac{t^6}{35} + \frac{t^8}{63} + O(t^{10})\right] \quad (3.3)$$

returning to the variable r, keeping only four nonzero terms of Taylor series and allocating the $1/r^2$ term we will obtain a simple equation describing the dose distribution at the distances sufficiently far from the GNP (several GNP radii):

$$D_1(r) = \frac{E_0}{4\pi\rho_w R_w} \frac{1}{r^2}\left[1 + \frac{R_{NP}^2}{5r^2} + \frac{3R_{NP}^4}{35r^4} + \frac{R_{NP}^6}{21r^6}\right]$$

$$D_1(r) = \frac{A}{r^2}\left[1 + \frac{R_{NP}^2}{5r^2} + \frac{3R_{NP}^4}{35r^4} + \frac{R_{NP}^6}{21r^6}\right] \quad (3.4)$$

where

$$A = \frac{E_0}{4\pi\rho_w R_w} \quad (3.5)$$

The constant A does not depend on the GNP radius and should be evaluated in $[nm^2]$ if substitute E_0 in $[J]$, ρ_w in $[kg/nm^3]$ and R_w in nm. For a 20 keV ejected photoelectron in water media $A = 2.98 \times 10^4\ nm^2$.

Figure 3.1 shows the deviation of the radial dose distributions from the $1/r^2$ law. The curves are the ratios of the dose distributions calculated for a GNP of radius 100 nm to the A/r^2 dependence. The upper curve (black) corresponds to the exact dose distribution Eq.(2.19) while the other curves are the approximate distributions Eq.(3.4) with increasing number of the Taylor terms. The straight line corresponds to the A/r^2 dependence. It is possible to see that sufficiently far from the GNP surface (more than $5R_{NP}$) the radial dose distribution follows to the $1/r^2$ dependence and is independent of the GNP radius.
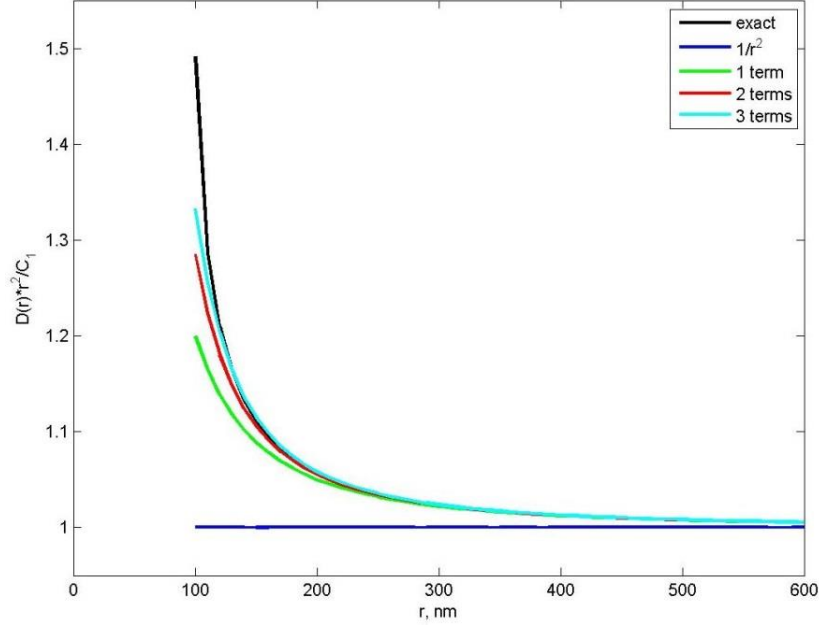
Figure 3.1 The deviation of the radial dose distribution around a GNP of radius 100 nm from the $1/r^2$ law. The curves are calculated as the ratio of the dose distribution to the A/r^2 dependence. . The upper curve (black) corresponds to the exact dose distribution Eq.(2.19). The other curves are the approximate distributions Eq. (3.4) with the indicated numbers of the Taylor terms. The straight line corresponds to the A/r^2 dependence.

During all the analysis we will try to maintain the radial dose deposition $D(r)$, as a general function, without specifying the dose dependence on the current distance from source in the GNP when exemplifications are suitable the first order approximation of Eq. (3.4) will be used for the radial dose deposition

$$D(r) = \frac{A}{r^2} \quad (3.6)$$

In the following, we will use the derived expressions in the previous chapter and as especial case of RDD the $1/r^2$ derived approximation to describe the dose distribution in an X-ray irradiated critical structure (cell) due to presence embedded gold nanoparticles (GNPs). For simplicity, the critical structure and GNP be considered as spheres of radii R_{st} and R_{NP}, respectively. We will suppose that the dose distribution around the GNP is spherically symmetric and described by a decreasing function $D(r)$.

The quantities $\bar{D}$ (average dose deposited in target) and $\overline{(D^2)}$ (average squared dose deposited in target) are calculated either in the special domain $d\vec{r}$ as an in the dose domain

dD, being the last a deduction with a higher physical meaning and a wider application due to no dependence on a specific dose deposition relation.

3.2 AVERAGE DOSE DISTRIBUTION IN A SPHERICAL CELL STRUCTURE DUE TO GNPS EXPERIENCING MULTIPLE IONIZATIONS; INTEGRATION IN THE SPATIAL DOMAIN.

Introducing a modification in the radial dose deposition expression proposed in Eq. (3.6) we can describe the dose around a nanoparticle as

$$D(r) = Dw\left(\frac{A}{r^2} + 1\right) \quad (3.7)$$

The first term of Eq. (3.7) is the dose deposition due to the presence of the GNP as a linear function on D_w, the second term is the prescribed dose to the whole system (macroscopic prescribed dose). To calculate the average dose in the volumes on radial dose deposition due to the GNP $\bar{D}_c$ (Average dose inside spheres of critical radius R_C surrounding each GNP) the following integral must be considered

$$\bar{D}_c = \frac{1}{V_C}\int_{|\vec{r}| \leq R_c} D(\vec{r})d\vec{r} \quad (3.8)$$

In the case of a single gold nanoparticle, centered in cell structure, and in virtue of the radial dose deposition expression, the expression (3.8) can be rewritten in spherical coordinates as

$$\bar{D}_c = \frac{1}{V_c}\int_0^{2\pi}\int_0^{\pi}\int_{R_{NP}}^{R_C} D(r)r^2\sin\theta\, dr\, d\theta\, d\phi \quad (3.9)$$

Introducing the proposed radial dose distribution (3.7) in (3.9)

$$\bar{D}_c = \frac{1}{V_c}D_w\int_0^{2\pi}\int_0^{\pi}\int_{R_{NP}}^{R_C}\left(\frac{A}{r^2} + 1\right)r^2\sin\theta\, dr\, d\theta\, d\phi$$

Introduce Eq. (3.7) imply that the dose deposition is isotropic around the nanoparticle after the ionizing events, due to the not dependence on the dose deposited in the angular coordinates, this integrals can be taken directly, obtaining

$$\bar{D}_c = \frac{4\pi}{V_c}D_w\int_{R_{NP}}^{R_C}\left(\frac{A}{r^2} + 1\right)r^2 dr$$

After integration the average dose deposited between R_{NP} and R_C

$$\bar{D}_c = \frac{3D_w}{R_c^3}\left(A(R_c - R_{NP}) + \frac{1}{3}\left(R_c{}^3 - R_{NP}{}^3\right)\right) \quad (3.10)$$

Following the same chain of procedures, to obtain the average quadratic dose deposited inside the regions R_c we have

$$\overline{(D^2)}_c = \frac{4\pi}{V_c}D_w{}^2\int_{R_{NP}}^{R_c}\left(\frac{A}{r^2} + 1\right)^2 r^2 dr$$

and after integration

$$\overline{(D^2)}_c = \frac{D_w{}^2}{R_{NP}R_cR_{st}{}^3}\left[-R_cR_{NP}{}^4 - 6AR_cR_{NP}{}^2 - 3A^2R_{NP} + R_{NP}R_c{}^4 + 6AR_{NP}R_c{}^2 + 3A^2R_c\right]$$

$$(3.11)$$

The expressions for R_c and A can be introduced in (3.11) and (3.10) to highlight the dependence of the expressions in the parameters, due to the extension of the equations these ones are not presented. Introducing the relative volume of water with dose equal to D_w as

$$Vrel_{D_w} = 1 - N_{GNP}\frac{R_c^3}{R_{st}^3} \quad (3.12)$$

being $Vrel_{D_w}$ the volume of the target outside the volumes of R_c surrounding each GNP. The average dose in the target can be rewritten (for the case of multiple gold nanoparticles in accomplished the condition of no overlapping radial dose deposition regions) as

$$\bar{D}_{targ} = \left(N_{GNP} \cdot \bar{D}_c + Vrel_{D_w} \cdot D_w\right) \quad (3.13)$$

The first term describing the average dose deposited in the critical volumes in the vicinity of the GNPs and the second term describing the average dose deposited in the volumes outside these regions, where the only dose deposited is the prescribed to the whole system. Introducing (3.10) and (3.12)

$$\bar{D}_{targ} = -\frac{D_w}{R_{st}^3}\left(N_{GNP}R_c^3 A - 3N_{GNP}AR_{NP} + 3N_{GNP}AR_c + R_{st}^3 - N_{GNP}R_{NP}^3\right)$$

$$(3.14)$$

Moreover the average quadratic dose deposited in the target $\overline{(D^2)}_{targ}$ can be written as

$$\overline{(D^2)}_{targ} = \left(N_{GNP} \cdot \overline{(D^2)}_c + Vrel_{D_w} \cdot D_w^2\right) \quad (3.15)$$

introducing (3.11) and (3.12)

$$\overline{(D^2)}_{targ} = \frac{D_w^2}{R_{NP}R_cR_{st}^3}\left(6N_{GNP}R_{NP}AR_c^2 - N_{GNP}R_cR_{NP}^4 - 6N_{GNP}R_cAR_{NP}^2 + 3N_{GNP}R_cA^2\right.$$
$$\left. - 3N_{GNP}R_{NP}A^2 + R_{NP}R_cR_{st}^3\right)$$

$$(3.16)$$

After introduce the dependence of the N_{GNP} in the mas concentration C_{Au} of GNPs and the dimensions of the target structure$N_{GNP}(C_{Au}, R_{st})$, the dependence of (3.14) and (3.16) in R_{st} disappear, therefore it is not a needed input parameter for the calculations.

3.3 THE DOSE DISTRIBUTION IN A CRITICAL STRUCTURE WITH SEVERAL GNPS FOR r^{-2} RADIAL DEPENDENCE; INTEGRATION IN THE DOSE DOMAIN.

Under the monotonic nature of the radial dose deposition, from (3.7) we can write an expression for r as a function of D.

$$r(D) = \sqrt{D_wA}(D - D_w)^{-\frac{1}{2}} \quad (3.17)$$

and

$$-\frac{dr(D)}{dD} = -(D_wA)^{\frac{1}{2}}\left(-\frac{1}{2}\right)(D - D_w)^{-\frac{3}{2}} = \frac{(D_wA)^{\frac{1}{2}}}{2(D - D_w)^{\frac{3}{2}}}$$

$$(3.18)$$

In general, the knowledge of GNP distribution inside and outside the critical structure is needed to calculate the dose distribution in a critical structure. It is follows from (3.7) that dose at distances sufficiently far from the GNP center is almost equal to the dose in water D_w. Recalling the introduction of a critical radius R_c at which the extra dose created by electrons ejected from a GNP is sufficiently small to compare with D_w. The Figure 3.2 presents the radial dose deposition around a 50nm GNP experiencing multiple ionizations (plot presents the radial dose deposition from the GNP surface).
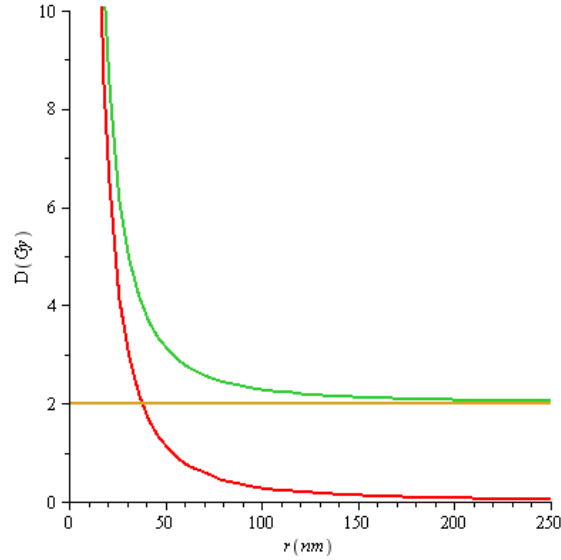
Figure 3.2 Radial dose deposition around a 50 nm gold nanoparticle suspended in water, irradiated isotropically with a monoenergetic beam of 100keV photons. The prescribed dose to the whole system (yellow line) is 2Gy, the red line is the radial dose deposition due to the GNP presence, and the green line is the total dose as described by Eq.(3.7)

Rewriting Eq.(2.40)

$$D(R_c) = D_w \left(\frac{A}{R_c^2} + 1 \right) = k_c D_w \quad (3.19)$$

where k_c is the coefficient (equal, for instance 0.1) specifying (quantifying) the condition $D(R_c) \ll D_w$.

The solution of (3.19) respect to R_c gives

$$R_c = \sqrt{\frac{A}{k_c}} \quad (3.20)$$

Fixing values for the incident photon energy and GNP radio, the distance at which the radial dose deposition due to GNP start to be negligible when compared to planed dose can be estimated .e.g. For a $50nm$ GNP irradiated with a $100kev$ photon beam and $k_c = 0.1\ D_w$ the R_c is about $72.19\ nm$.

In the case of homogenous distribution of GNPs inside the critical cell the average distance between GNPs is determined by the expression (Hetz & Chandrasekhar, 2011)

55

$$l_{av} = \Gamma\left(\frac{4}{3}\right)\left(\frac{3}{4\pi n_{NP}}\right)^{\frac{1}{3}} \approx 0.544(n_{NP})^{-\frac{1}{3}} \quad (3.21)$$

Where Γ is the gamma function and n_{NP} is the concentration of GNPs in the critical target.

The condition

$$R_c \ll l_{av} \text{ or } n_{NP} \ll \left(0.554\sqrt{\frac{A}{k_c}}\right)^3 \quad (3.22)$$

determines the maximal GNP concentration, at which the volumes of no negligible radial dose deposition due to individual GNPs (spheres of radii R_c) are not overlapped. Therefore, we can summaries the volumes $dV(D)$ corresponding to given doses between D and $D + dD$ and express the dose distribution function in the case of several GNPs in the target as

$$p(D) = \frac{N_{GNP}R_{NP}^3}{R_{st}^3}\delta(D) + \left(1 - \frac{N_{GNP}R_C^3}{R_{st}^3}\right)\delta(D - D_w), \quad 0 \leq D \leq D_w\left(\frac{A}{R_{st}^2} + 1\right)$$

$$p(D) = N_{GNP}\frac{3(D_wA)^{\frac{3}{2}}}{2R_{st}^3(D - D_w)^{\frac{5}{2}}}, \quad D_w\left(\frac{A}{R_{st}^2} + 1\right) \leq D \leq D_w\left(\frac{A}{R_{NP}^2} + 1\right)$$

$$p(D) = 0, \quad D \geq D_w\left(\frac{A}{R_{NP}^2} + 1\right)$$

(3.23)

The first term in (3.23-1) takes into account the total volume of GNPs with the dose supposed to be equal to 0 (it does not participate in the dose deposition in cell), the second term represents the dose in the regions of target outside the volumes of critical radii and the Eq. (3.23-2) presents the dose deposition due to GNPs inside the volumes of critical radii. The total volume of the target with dose D_w (represented in the second term of the equation).

Proposing the radial dose distribution in the target in a vicinity of GNP ($r \leq R_c$) as follows

$$D_{st} = \frac{D_w \cdot A}{r^2} + D_w$$

$$D_{min} = \frac{D_w \cdot A}{R_c^2} + D_w$$

$$D_{max} = \frac{D_w \cdot A}{R_{NP}{}^2} + D_w$$

(3.24)

The average doses in target can be calculated for the case of multiple GNP without overlapping regions as

$$\overline{D}_{st} = \int_0^{D_{min}} D \cdot p_1(D).\, dD + \int_{D_{min}}^{D_{max}} D \cdot p_2(D).\, dD$$

(3.25)

Where the sub-script represent the first and second equations of Eq.(3.23) , Eq.(3.25) can be divided in two parts the first integral recalled as $\overline{D}_{st_\delta}$ representing the average dose deposited inside the GNPs and the regions outside the R_c. The second integral named $\overline{D}_{st_{GNP}}$ describing the average dose deposited inside the regions of R_c. Rewriting the first part of (3.25) introducing the expression for $p_1(D)$ from (3.23-1) we obtain

$$\overline{D}_{st_\delta} = \int_0^{D_{min}} D \cdot p_1(D).\, dD = \int_0^{D_{min}} D \cdot \left[\frac{N_{GNP} R_{NP}^3}{R_{st}^3} \delta(D) + \left(1 - \frac{N_{GNP} R_C^3}{R_{st}^3}\right)\delta(D - D_w)\right] dD$$

(3.26)

and after integration Eq.(3.26) reduces to

$$\overline{D}_{st_\delta} = D_w \left(1 - \frac{N_{GNP} R_c^3}{R_{st}^3}\right) \quad (3.27)$$

The second part of (3.25) introducing the expression for $p_2(D)$ from (3.23-2) can be rewritten as

$$\overline{D}_{st_{GNP}} = \int_{D_{min}}^{D_{max}} D \cdot p_2(D).\, dD = D_{av_\delta} = \int_{D_{min}}^{D_{max}} D \cdot N_{GNP} \frac{3(D_w A)^{\frac{3}{2}}}{2 R_{st}^3 (D - D_w)^{\frac{5}{2}}} dD$$

(3.28)

The integration results

$$\overline{D}_{st_{GNP}} = \frac{D_w \cdot N_{GNP}}{R_{st}^3}\left[\left(1 + \frac{3A}{R_c^2}\right)R_c^3 - \left(1 + \frac{3A}{R_{NP}^2}\right)R_{NP}^3\right]$$

(3.29)

The addition of the results after integration of Eq.(3.27) and Eq.(3.29) is the total average dose in the target structure

$$\overline{D}_{st} = \overline{D}_{st_{\delta}} + \overline{D}_{st_{GNP}}$$

$$\overline{D}_{st} = D_w\left(1 - \frac{N_{GNP}R_c^3}{R_{st}^3}\right) + \frac{D_w \cdot N_{GNP}}{R_{st}^3}\left[\left(1 + \frac{3A}{R_c^2}\right)R_c^3 - \left(1 + \frac{3A}{R_{NP}^2}\right)R_{NP}^3\right]$$

(3.30)

The same chain of calculations can be done to obtain the average squared dose defined as

$$\overline{(D^2)}_{st} = \int_0^{D_{min}} D^2 \cdot p_1(D). \, dD + \int_{D_{min}}^{D_{max}} D^2 \cdot p_2(D). \, dD$$

(3.31)

Splitting the previous equation in two terms; the first part can be rewritten as

$$\overline{(D^2)}_{st_{\delta}} = \int_0^{D_{min}} D^2 \cdot p_1(D). \, dD = \int_0^{D_{min}} D^2 \cdot \left[\frac{N_{GNP}R_{NP}^3}{R_{st}^3}\delta(D) + \left(1 - \frac{N_{GNP}R_c^3}{R_{st}^3}\right)\delta(D - D_w)\right] dD$$

(3.32)

The integration of (3.32) is

$$\overline{(D^2)}_{st_{\delta}} = D_w{}^2\left(1 - \frac{N_{GNP} \cdot R_c^3}{R_{st}^3}\right) \quad (3.33)$$

and the second part of (3.31)

$$\overline{(D^2)}_{st_{GNP}} = \int_{D_{min}}^{D_{max}} D^2 \cdot p_2(D). \, dD = \int_{D_{min}}^{D_{max}} D^2 \cdot N_{GNP}\frac{3(D_w A)^{\frac{3}{2}}}{2R_{st}^3(D - D_w)^{\frac{5}{2}}}dD$$

(3.34)

The result of the integration Eq.(3.34) is

$$\overline{(D^2)}_{st_{GNP}} = \frac{N_{GNP} D_w{}^2}{R_{st}^3} \left[\left(8 - 12 \left(\frac{A}{R_{NP}^2} + 1 \right) + 3 \left(\frac{A}{R_{NP}^2} + 1 \right)^2 \right) R_{NP}^3 \right.$$

$$\left. - \left(8 - 12 \left(\frac{A}{R_C^2} + 1 \right) + 3 \left(\frac{A}{R_C^2} + 1 \right)^2 \right) R_C^3 \right]$$

(3.35)

As previously Eq. (3.33) describe average squared dose inside the nanoparticle and the dose outside the critical radius; and Eq.(3.35) describe the average squared dose due to the GNP presence, deposited inside the volume of critical radius. After integration and adding (3.33) with (3.35) we obtain the total average squared dose

$$\overline{(D^2)}_{st} = \overline{(D^2)}_{st_\delta} + \overline{(D^2)}_{st_{GNP}}$$

$$\overline{(D^2)}_{st} = D_w{}^2 \left[\left(1 - \frac{N_{GNP} \cdot R_C^3}{R_{st}^3} \right) \right.$$

$$+ \frac{N_{GNP}}{R_{st}^3} \left[\left(8 - 12 \left(\frac{A}{R_{NP}^2} + 1 \right) + 3 \left(\frac{A}{R_{NP}^2} + 1 \right)^2 \right) R_{NP}^3 \right.$$

$$\left. \left. - \left(8 - 12 \left(\frac{A}{R_C^2} + 1 \right) + 3 \left(\frac{A}{R_C^2} + 1 \right)^2 \right) R_C^3 \right] \right]$$

(3.36)

Equations (3.30) and (3.36) are going to be used in the analysis of cell survival from the perspective of the dose domain dD in the following chapter. As expected the average dose and average squared dose calculated by the two different special approaches (r or D) lead to the same results, evidencing the equivalence of the descriptions developed in the two different approaches.

CHAPTER IV. AN APLICATION OF THE DOSE DEPOSITION IN CRITICAL STRUCTURES: CELL SURVIVAL CALCULATIONS.

4.1 GENERAL ASPECTS OF RADIATION DAMAGE TO CELLS AND TISSUES.

Studies of the biological action of ionizing radiation on cells and tissues are of interest for applications in radiotherapy as well as radiation protection. When discussing the biological action of radiation – whether due to photon, electron or ion beams – on living cells and tissue, several differences to the action on non-living material have to be considered. Processing of damage includes a whole spectrum of possible reactions, repair of the damage being the most important one. Processing of damage takes time, and in combination with other kinetic effects it thus implies a pronounced time dependence of biological effects, spanning a huge time scale from minutes to years until the primary induced damage is actually converted into a visible or detectable biological response. Furthermore, the radiation response of tissues is characterized by a complex interplay between different cells types, each of them showing an individual response to radiation damage.

The above mentioned processes play an important role for the interpretation and understanding of the dose response curves observed after irradiation, which may vary considerably depending, for example, on the particular cell type, environmental conditions and the time structure of dose delivery.

A single cell represents the smallest functional unit of any complex organized tissue. In general, within a single cell two clearly separated compartments can be distinguished visually and functionally: the cell nucleus and the cytoplasm. The cell nucleus contains the genetic information in form of a large macromolecule, the Deoxyribonucleic Acid (DNA). In combination with additional proteins secondary, tertiary and higher-order structures are built, resulting in a condensed structure of the DNA molecule.

Within the cytoplasm, further substructures (organelles) can be distinguished. All of them are separated by membranes, which allow to keep concentration gradients of certain types of ions or molecules. This is also true for the outer cell membrane, separating the inner cell

volume from the environment. A typical characteristic of many cells is their ability to grow and to produce two identical daughter cells by cell division. This division requires the exact duplication of the DNA contained in the cell nucleus, and the precise distribution of each of the two copies into the daughter cells. The total time for a complete division cycle of typical mammalian cells under laboratory conditions is in the order of 12–24 hours.

Starting from the structural complexity of a single cell, the question arises, which compartment is most sensitive to radiation and can thus be expected to be responsible for the observable response of a cell to radiation. Experimental results have demonstrated a correlation between the radiosensitivity and the DNA content, at least for groups of biologically similar objects: the higher the amount of DNA, the more sensitive the object. These results already suggested the DNA to play a key role in the response to radiation. This hypothesis was proven also more directly for mammalian cells. The experiments revealed, that energy deposition in the nucleus is by far more efficient to produce biological damage, compared to the case where similar amounts of energy are deposited to the cytoplasm only. However, there is increasing evidence in the last few years, that DNA damage is not necessarily a prerequisite for the induction of biologically relevant effects.

Lesions do not necessarily occur separately, but instead, depending on the dose level, combinations of different types occurring in close vicinity can lead to more complex lesions. Since the information on both strands of the DNA molecule is complementary, all injuries affecting only one side of the DNA double strand like, for example, single strand breaks (SSB) can be potentially easily repaired by using the information on the intact strand as a template. Therefore, double strand breaks (DSB) are generally considered as the critical event for the induction of lethal lesions. The incidence of several types of lesions after application of $1\ Gy$ to a typical cell are presented in Table 4.1. These numbers, however, should only illustrate an order of magnitude; there can be considerable variations from cell type to cell type. (Scholz, 2006)

Approximate yields of DNA damage per Gy per cell	
SSB	1000
DSB	30–40
DNA–Protein crosslinks	50
Complex damage (SSB + Base lesion)	60

Table 4.1 Stimation of the number of each tipe of lesions after the irradiation of 1Gy to a typical cell.

4.1.1 Cell survival essays.

Investigation of radiation induced cell death, defined as mitotic death in the sense of a complete loss of the proliferation capacity, is one of the most commonly used methods to study radiation effects on cells. As mentioned earlier, many cell types are characterized by regular cell division in 12–24 h intervals. Thus, according to the exponential growth, a single cell can produce thousands of daughter cells within a few days. If the cells are originally seeded in culture flasks at the appropriate low density, the daughter cells of each individual cell appear as clusters or 'colonies'. A cell is classified as 'survivor', if it is able to produce at least 50 daughter cells within a time interval of approximately 10–14 normal division cycles, i.e. 5–14 days; if less than 50 daughter cells are produced, the cell is classified as dead or 'inactivated' (Puck and Markus, 1956). The threshold of 50 cells is an empirically determined value and somewhat arbitrary.

Most experiments to study survival probabilities are based on a so called dilution assay Figure 4.1, which briefly consists of the following steps

• After irradiation, a cell suspension is produced by removing the cells grown on the bottom of the culture vessel by controlled enzymatic digestion. The cell number in the suspension is counted.

• From the dose delivered, the expected fraction of surviving cells is estimated. The cell suspension is then diluted and aliquots are reseeded to new culture vessels at a density, that approximately 100 surviving cells are expected per culture vessel.

• Cells are incubated for 5–14 days typically, corresponding to 10–14 cycle times.

• The number of colonies with more than 50 cells is determined; the fraction of surviving cells is then calculated by normalization to the number of cells originally seeded in the flask.
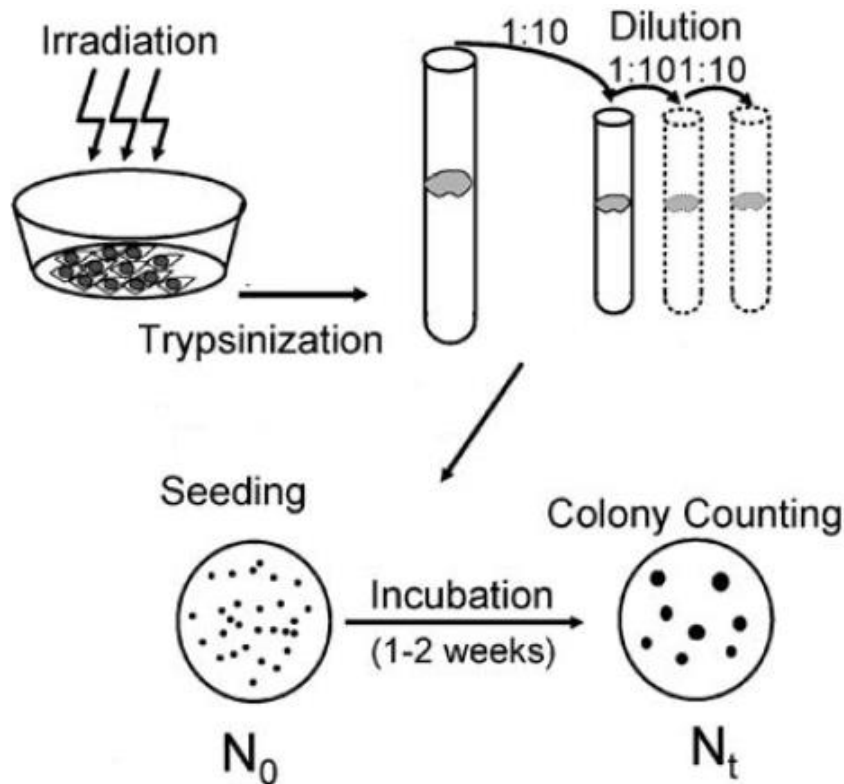

Figure 4.1 Dilution assay for measuring cell survival after irradiation. Adapted from *(Scholz, 2006)*

Cellular survival as a function of dose follows almost exponential behavior, and thus survival curves are generally shown in logarithmic plots. A purely exponential behavior would be expected based on simple mechanistic assumptions on the distribution of energy deposition and damages. The most prominent feature of most survival curves is thus the deviation from such a simple curve, namely, the dose response curve typically shows a shoulder. For most cell types, survival curves start with a moderate slope, and with increasing dose, the slope correspondingly increases.

Therefore, the efficiency per dose increment increases as well. This can be understood in terms of the reparability of radiation induced damages. At low doses, only a few damages are induced with a large spatial separation, and a considerable fraction of these damages can be repaired correctly. In contrast, at high doses, the density of damages increases, leading to an interaction of damages and thus a reduced fraction of repairable damages. The term 'interaction' has to be understood here in the most general sense. It can happen, that actually two individual damages are combined to form a more complex type of damage; on the other hand, two damages produced in close vicinity can lead to conflicting or competing repair processes, also reducing the fraction of repairable damage. The following sub chapter present an analytical description of the cell survival response modifications of cell cultures with embedded GNPs after irradiation. The perspective is presented from the view of the dose space of radial dose deposition with the proposed relations obtained in chapter 3.

4.2 AN APPLICATION OF THE DOSE DEPOSITION IN CRITICAL STRUCTURE; CELL SURVIVAL FROM THE DOSE DOMAIN.

The number of lesions in the target due to the presence of multiple nanoparticles can be obtained with the following equation (Zygmanski, et al., 2013)

$$NL_{tot} = \int_0^\infty (\alpha D + \beta D^2) p(D) dD \quad (4.1)$$

Eq.(4.1) can be splitted in two parts one averaging the number of lesion in a linear dose dependence and the other averaging the number of lesions in a quadratic dose dependence as

$$NL_{lin} = \alpha \int_0^\infty D \, p(D) dD$$

$$NL_{qua} = \beta \int_0^\infty D^2 p(D) dD$$

$$(4.2)$$

The two equations presented in (4.2) are actually the average dose $\bar{D}_{st}$ and the average squared dose $\overline{(D^2)}_{st}$ presented in the calculations of chapter III. Eq. (3.30) and (3.36), therefore the total number of lesion in target can be written as

$$NL_{tot} = \alpha \bar{D}_{st} + \beta \overline{(D^2)}_{st} \quad (4.3)$$

The evaluation of the integrals in Eq.(4.2-1) evidence the linear dependence of $\bar{D}_{st}$ in D_w, and in the same way the evaluation of the integral in Eq.(4.2-2) stick out the squared dependence of $\overline{(D^2)}_{st}$ in D_w. Specifying the average number of lesions in the target due to the linear part (first part of Eq.(4.3))

$$Nlin_{tar} = \alpha D_w \left[\left(1 - \frac{N_{GNP} R_c^3}{R_{st}^3} \right) + \frac{N_{GNP}}{R_{st}^3} \left\{ \left(1 + \frac{3A}{R_c^2} \right) R_c^3 - \left(1 + \frac{3A}{R_{NP}^2} \right) R_{NP}^3 \right\} \right]$$

$$(4.4)$$

and specifying the average number of lesion in target due to the quadratic part (second term in Eq. (4.3))

$$Nqua_{tar} = \beta D_w^2 \left\{ \left(1 - \frac{N_{GNP} R_c^3}{R_{st}^3} \right) \right.$$

$$+ \frac{N_{GNP}}{R_{st}^3} \left[\left(8 - 12 \left(\frac{A}{R_{NP}^2} + 1 \right) + 3 \left(\frac{A}{R_{NP}^2} + 1 \right)^2 \right) R_{NP}^3 \right.$$

$$\left. - \left(8 - 12 \left(\frac{A}{R_c^2} + 1 \right) + 3 \left(\frac{A}{R_c^2} + 1 \right)^2 \right) R_c^3 \right] \right\}$$

$$(4.5)$$

Therefore after replacing the specific dependences in equation (4.3) the equation can be rewritten in terms of modified coefficients α and β. Therefore (4.3) can be rewritten as

$$NL_{tot} = \alpha_{GNP} D_w + \beta_{GNP} D_w^2 \quad (4.6)$$

Where α_{GNP} and β_{GNP} are the response parameter of the cell culture with embedded GNP exposed to the same irradiation as when α and β where evaluated in the biological essay. The modified response parameters are obtained after evaluate all the quantities in A, N_{GNP}, R_c and specify the values of the mass concentration C_{Au} and the GNPs radius. All the numerical values can be collected in this new coefficients α_{GNP} and β_{GNP}, maintaining the linear quadratic dependence in D_w. (The radius of the target structure is not a needed parameter, R_{st} disappear of the expressions after introduce the N_{GNP} as a function of the mass concentration C_{Au} and the structure radius R_{st}).

Being as in the L.E.M the survival probability

$$S = e^{-\alpha_{GNP} \, Dw - \beta_{GNP} Dw^2} \quad (4.7)$$

We have obtained a form of assess the response of a cell culture with embedded GNPs, taken as an input the parameters that characterize its response when irradiated without GNPs, the characteristics of the GNP and characterization of the irradiation process.

The same calculation can be made in the spatial domain r with the local effect model (LEM). For inhomogeneous radiation, the number of lesions induced is calculated based off the local dose at each point and then integrated over the whole cell volume, giving

$$NL_{tar} = \int N(D(r)) \frac{dV}{V} = \int (\alpha D(r) + \beta D(r)^2) \frac{dV}{V}$$

(4.8)

And the surviving fraction is

$$S = e^{-NL_{tar}} \quad (4.9)$$

The integrals in Eq.(4.8) were presented in the third chapter Eq.(3.14) an Eq. (3.16) after some algebra we obtain the same results that for the average dose deposited an average quadratic dose deposition in the dose domain D Eq. (3.30) and Eq.(3.36). Therefore we have obtain the same cell response from the two different perspectives (the same number of lesions in target and the same survival fraction). This fact allow us to trust in the veracity of our proposed model.

 The obtained results are presented in the following section.

4.2.1 Obtained results for Cell survival.

With the goal of estimate results of the analytical scheme presented previously Chapter 4.2. The cell line MDA-MB-231 human mammary gland/breast cells has been chosen, characterized for the $\alpha = 0.019\ [1/Gy]$ and $\beta = 0.052\ [1/Gy^2]$ responding to a $160kVp$ photon source (Jain, et al., 2011). Figure 4.2 presents the cell survival modified response of the cell culture when it had embedded $1.9nm$ GNPs and is exposed to the same planed radiation treatment.
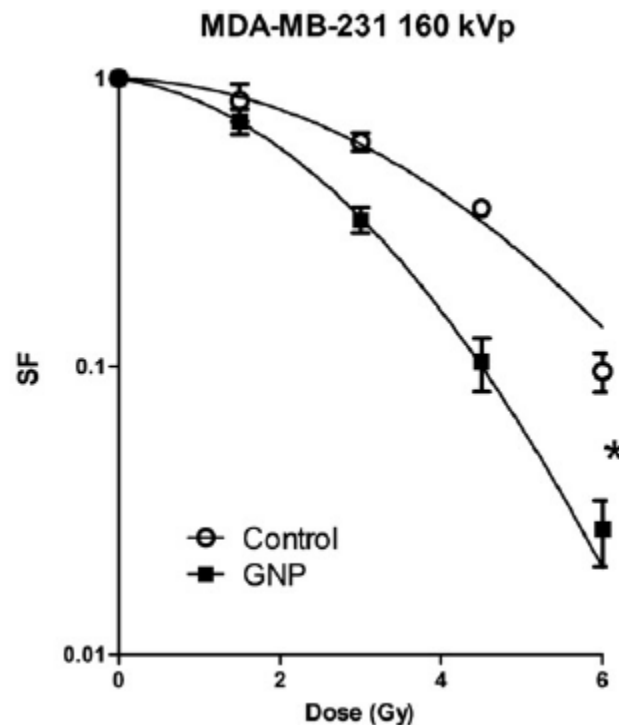

Figure 4.2 Radiation dose response curve for MDA-MB-231 cell line with GNPs irradiated with 160kVp x-rays containing $0\frac{\mu g}{mL}$ (☉) and $2.85\frac{\mu g}{mL}$ (■) gold nanoparticles. Adapted from *(Jain, et al., 2011)*

With the help of the software Maple 12. Numerical evaluation of the expression obtained in the sub chapter 4.2 can be performed, to fulfil this aim all the parameters should be replaced by its numerical value; it is important in each procedure corroborate the dimension concordance of the variable assessed. In this particular evaluation, for the equation (4.7), the following described values had been assigned to each coefficient:

- Initial energy of an incident photon in J; $E_p = 1.602 x 10^{-14} J$

- The energy of photoelectron in J; $K_{Epe} = 3.204 x 10^{-15} J$

- CSDA ranges of photoelectron of energy 20 keV in water and gold, respectively, in nm $R_{Au} = 1170nm$; $R_w = 8570nm$.

- The photoelectric effect probability for 100 keV photons; $K_{pe} = 0.94$

- The probability for the photoelectric effect at K shell; $P_K = 0.801$

- The mass attenuation coefficient of gold and the mass energy-transfer coefficient of water for 100 keV photon, in cm^2/g; $\frac{\mu_{en}}{\rho}\bigg|_{Au} = 5.158 \frac{cm^2}{g}$, $\frac{\mu_{tr}}{\rho}\bigg|_w = 0.02546 \frac{cm^2}{g}$ respectively.

- The radius of the R_{NP} GNP, in nm ; $R_{NP} = 100nm$

- The GNP concentration in target C_{Aa}, in mg/g; $C_{Aa} = 7\frac{mg}{g}$

- The α, β coefficients for the cell culture irradiated with the prescribed dose of x-rays $\alpha = 0.019\,[1/Gy]$ and $\beta = 0.052\,[1/Gy^2]$

After replace those values in the set of equations Eq.(3.30)-Eq.(3.36), the cell survival curve obtained for the cell culture with embedded $100nm$ GNP is presented in Figure 4.3
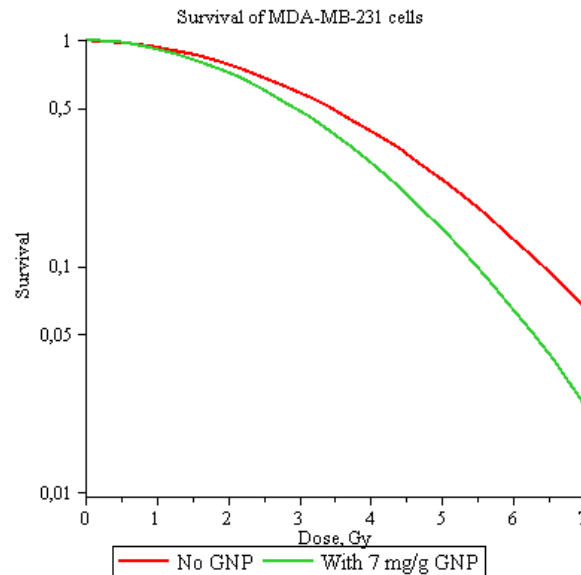

Figure 4.3 Survival curve for MDA-MB-231 cells exposed to a 100 keV x-ray irradiation, red line cell without nanoparticles, green line cell with embedded 100 nm GNP.

The obtained parameters following the calculations are $\alpha_{GNP} = 0.02128$ and $\beta_{GNP} = 0.07264$; and the reported ones $\alpha r_{GNP} = 0.091$ $\beta r_{GNP} = 0.093$; results are not the same, but maintain a good agreement between them. The differences in results was expected due to the differences between the irradiation essay and the calculated one; e.g. the differences in the energies of the photon beam; the radii of the considered nanoparticles and the concentration in target. Improvements to reproduce the experimental essays can be done, but we consider it a failed effort, due to the lack of exact information of the papers that report experimental results in terms of GNPs localization and GNPs uptake by cells.

The Figure 4.4 presents the modifications in the response of the cell culture to varying concentration of GNPs. As expected when the concentration increases the fraction of survival cells decrease for the same scheme of irradiation, the variation in the response is remarkable at higher doses.
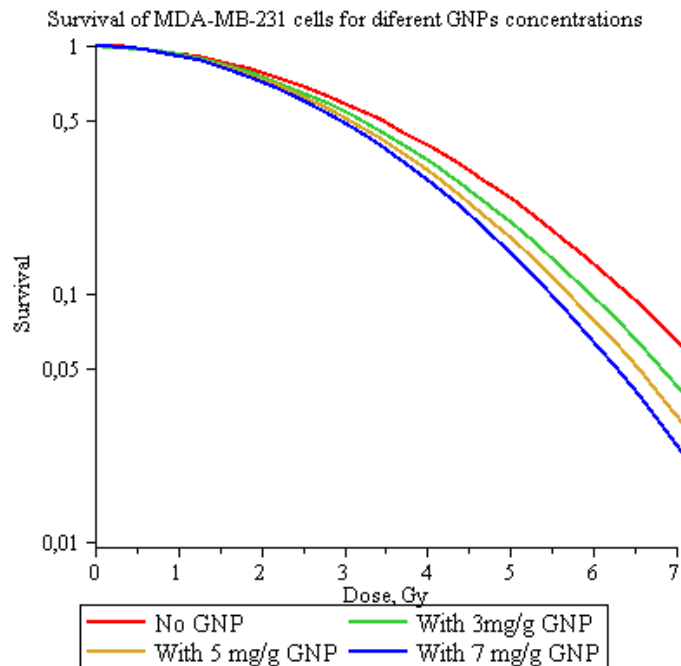

Figure 4.4 Calculated Survival fraction for MDA-MB-231 cells for different GNPs concentrations. The input parameters are mantained as in Figure 4.3

CONCLUSIONS

- A literature review of the applications of GNPs as radiosensitizers in radiotherapy was sketched, highlighting the viability of further developments in cancer treatments as GNP aided radiotherapy, proposed for various authors. The review of the models that describe cell survival experiments was also performed, recalling the parameters, taking into consideration, and presenting the LEM model as the more suitable to describe the radiosensitization effect of GNPs embedded in cell cultures.

- The general framework starting from the irradiation process to the assessment of the dose deposition in a critical structure with embedded GNPs was developed. The proposed framework is a general analytical approach that admits arbitrary radial dependence of the dose delivered from the GNPs.

- In order to perform estimations, a simple expression ($1/r^2$ dependence) for the radial dose deposition around a single GNP suspended in water-like tissue after irradiation has been proposed, which satisfactory fits the obtained general expression.

- Two main suppositions to derive close analytical formulas were proposed: the isotropic and homogenous irradiation of the GNPs with photons resulting in isotropic radial dose distribution around GNP and sufficiently low GNP concentration in the target allowing to exclude from consideration the extremely complex case of overlapping dose enhanced regions around individual GNPs. Each one of this can be modified in order to present a more realistic frame, but to provide these modifications information about the angular dependence of the radial dose distribution and a method to take into account dose overlapping from different GNPs are needed.

- Exact knowledge about the number of GNP inside a cell structure and its specific location in the main structures of the target is not available at nowadays stage of the research in GNP uptake into mammalian cells. Therefore, we had proposed an simplify framework to assess cell survival that that does not need such information

and has as parameters the weight concentration of nanoparticles per unit volume of the cell structure and the GNP radius, parameters that can be well determined in experimental essays.

- The average dose and average squared dose in a target structure with homogeneously distributed GNPs were calculated by the two different approaches (spatial r-domain and dose D-domain) both leading to the same results, evidencing the equivalence of the descriptions. Furthermore, we have obtained the same cell response from the two different integration domains (the same number of lesions in target and the same survival fraction). This fact confirms the veracity of the proposed approach.

- The analytical approach to assess cell survival was compared with experimental results reported in literature, the calculated survival curves present a good agreement with the reported experimental ones; the fraction of cells surviving under the same prescribed treatment decrease when they had embedded GNPs, and the effects are more appreciable when the mass concentration of GNPs increases in a target. Specific experimental essays are necessary in order to assess the coincidence of our analytical approach with experimental results.

BIBLIOGRAPHY

Attix, F. (2004). *Introduction to radiological physics and radiation dosimetry* . Weinheim : WILEY-VCH.

Ballarini, F. (2010). From DNA Radiation damage to cell death: Theoretical approaches. *Journal of Nucleic Acids*.

Berbeco, R., Ngwa, W., & Makrigiorgos, M. (2011). Localized dose enhancement to tumor blood vessel endothelial calls via megavoltage x-rays and targeted gold nanoparticles: new potential for external beam radiotherapy. *Int. J. Radiation Oncology Biol. Phys.*, 270-276.

Chernov, G. (2014). *Nanoscale dose distribution around a gold nanoparticle embedded in water (an analytical approach). MSc thesis.* Hermosillo, Sonora: Universidad de Sonora.

Chernov, V., Chernov, G., & Barboza-Flores, M. (2012). Analytical approximation of the nanoscale dose distribution in an irradiated medium with an embedded nanoparticle. *Journal of Physics: Conference Series*, 1-5.

Chithrani, B., Chazani, A., & Chan, W. (2006). Determining the size and sahape dependence of gold nanoparticles uptake into mammalian cells. *Nano letters*, 662-668.

Cho, S., Jones, B., Krishman, & Sunil. (2009). The dosimetric feasibility of gold nanoparticles-aided radiation therapy (GNRT(via brachyterapy using low-energy gamma- / x-rays sources. *Physics in Medicine and Biology.*, 4884-4905.

Elsässer, T., & Scholz, M. (2007). Cluster effects within the local effect model. *Radiation Research*, 319-329.

ESTAR, N. I. (2012). *Stopping-power and range tables for electrons*. Retrieved from http://physics.nist.gov/PhysRefData/Star/Text/ESTAR.html

Goddlu, S., Houell, W., & Rao, D. (1994). Cellular dosimetry: Absorbed fractions for monoenergetic electron and alpha particle sources and s-values for radionuclides uniformly distributed in different cell compartments. *J. Nucle. Med*, 303-316.

Herold, D., Das, I., Stobbe, C., Iyer, R., & Champman, J. (2000). Gold microspheres: a selective technique for producing biological effective dose enhancement. *International Journal of radiation biology*, 1357-1364.

Hetz, P., & Chandrasekhar, S. (2011, March 3). *Mean inter-particle distance.* Retrieved from http://en.wikipedia.org/wiki/Mean_inter-particle_distance

Hossain, M., & Su, M. (2012). Nanoparticle location and material-dependent dose enhancement in x-ray radiation therapy. *The journal of physical chemestry C*, 23047-23052.

ICRU85, R. (2011). *Fundamental quantities and units for ionizing radiation (revised).* Oxford University Press.

Jain, S., Coulter, J., Hounsell, A., Butterworth, K., McMahon, S., Hyland, W., . . . Hirst, D. (2011). Cell-Specific radiosensitization by gold nanoparticles at megavoltage radiation energies. *International Journal of Radiation Oncology Biol. Phys.*, 531-539.

Kobayashi, K., Usami, N., Porcel, E., Lacombe, S., & Sech, C. (2010). Enhancement of radiation effect by heavy elements. *Mutation research*, 123-130.

Lechtman, E., Chattopadhyay, N., Cai, Z., Mashouf, S., Reilly, & Pignol, J. (2011). Implications on clinical scenario of gold nanoparticle radiosensitization in regards to photon energy, nanoparticle size, concentration and location. *Physics in medicine and biology*, 4631-4647.

Lehnert, S. (2007). *Biomolecular action of ionizing radiation.* Danvers: Taylor & Francis Group.

McMahon, S., Hyland, W., Muir, M., Coulter, J., Jain, S., Butterworth, K., . . . Currel, F. (2011). Biological consequences of nanoscale energy deposition near irradiated heavy atom nanoparticles. *Scientific Reports*, 1-8.

McMahon, S., Hyland, W., Muir, M., Coulter, J., Jain, S., Butterworth, K., . . . Currell, F. (2011). Nanodosimetric effects of gold nanoparticles in megavoltages radiation therapy. *Radiotherapy and Oncology*, 412-416.

McParland, B. J. (2010). *Nuclear medicine radiation dosimetry.* Amersham. United Kingdom: Springer.

Ngwa, W., Makrigiorgos, G., & Berbeco, R. (2010). Applying gold nanoparticles as tumor-vascular disrupting agents during brachytherapy: estimation of endothelial dose enhancement. *Physics in Medicine and Biology*, 6533-6548.

Ngwa, W., Makrigiorgos, M., & Berbeco, R. (2012, January). Gold nanoparticle-aided brachytherapy with vascular dose painting: Estimation of dose enhancement to the tumor endothelial cell nucleus. *Medical Physics, 39*(1), 392-398.

Rahman, W. N. (2010). *Gold Nanoparticles: Novel radiobiological dose enhancement studies for radiation therapy, synchroton based microbeam and sterotactic raditherapy.* RMIT University.

Scholz, M. (2006). *Microdosimetric response of physical and biological systems to low-and high-LET radiations: Theory and applications to dosimetry.* Darmstadt: Elsevier B.V.

Zygmanski, P., Hoegele, W., Tsiamas, P., Cifter, F., Ngwa, W., Berbeco, R., . . . Sajo, E. (2013). A stochastic model of cell survival for high-Z nanoparticle radiotherapy . *Medical Physics* , 1-16.

Zygmanski, P., Liu, B., Tsiamo, P., Cifter, F., Petersheim, M., Hesser, J., & Sajo, E. (2013). Dependence of monte carlo microdosimetric computations on the simulation geometry of gold nanoparticles. *Phys. Med. Biol.*, 7961-7977.